Title

Hyperfine Interactions and Molecular Motion of the Mu−Ethyl Radical in Faujasites: NaY, HY, and USY

Journal

The Journal of Physical Chemistry C, 111(27)

ISSN

1932-7447

Authors

Bridges, Michael D
Arseneau, Donald J
Fleming, Donald G
et al.

Publication Date

2007-07-01

DOI

10.1021/jp0686341

Hyperfine Interactions and Molecular Motion of the Mu−Ethyl Radical in Faujasites: NaY, HY, and USY

Michael D. Bridges,[†] Donald J. Arseneau, Donald G. Fleming,*[,‡] and Khashayar Ghandi[§]

TRIUMF and Department of Chemistry, University of British Columbia, Vancouver, British Columbia V6T 2Z1, Canada

Received: December 15, 2006; In Final Form: April 1, 2007

The adsorption and dynamical behavior of the Mu−ethyl radical (MuC_2H_4) in NaY, HY, and USY faujasites was investigated by the muon spin resonance (μSR) technique, at loadings of one to five ethene molecules per supercage and over a temperature range of ca. 5−500 K (for NaY). The temperature dependences of both the muon and proton hyperfine coupling constants (Hfc's) are reported and compared with similar studies of MuC_2H_4 in different environments. Both transverse field (TF) μSR and avoided level crossing resonance (ALC) μSR spectra were recorded, with information on molecular motion mainly provided by the ALC line shapes. The muon Hfc's show only a small sensitivity to different frameworks and loadings but exhibit significant (∼10%) shifts at low temperatures, in comparison with bulk values, due to binding of the ethyl radical to cations at S_{II} sites in NaY and to framework hydroxyls in the case of HY(USY). The Δ_1 resonances are symmetric and quite broad at the lower temperatures studied, but dramatically further broaden near room temperature, seen also in the TF relaxation rates, suggesting that the Mu−ethyl radical either desorbs from or hops between its binding sites at the higher temperatures. An Arrhenius estimate of the activation energy for desorption gives ∼ 20 kJ/mol, consistent with the dipolar interaction energy between the Mu−ethyl radical and an NaY cluster. The observation of such highly broadened Δ_1 ALC lines at the higher temperatures contrasts with the largely static line widths reported previously for the Mu−cyclohexadienyl radical (MuC_6H_6) in NaY. Sharper Δ_0 ALC lines for both the α and β protons of MuC_2H_4 appear near the same temperatures at which the Δ_1 lines overly broaden, and which persist to the highest temperatures (350 K). For NaY, the α proton resonances also broaden further at these temperatures. For both NaY and particularly HY, the temperature dependence of the α proton Hfc's indicates considerable distortion of the Mu−ethyl radical geometry, due to its binding to zeolite sites. Recently published calculations of binding energies and Hfc's for ethyl radicals in NaY and HY suggest a much stronger binding of the MuC_2H_4 radical than seems warranted by the data and pose as well a conundrum in comparison with earlier results for MuC_6H_6 in NaY. On the other hand, the temperature dependence of the isotropic muon Hfc's found from the T-atom model for NaY employed in these calculations is in excellent agreement with experiment.

1. Introduction

Despite the well-known importance of zeolites as catalysts in particularly the petrochemical industry,[1−6] there is surprisingly little understanding of the nature of the interactions involved in catalytic steps at a molecular level. Proton-transfer reactions to organic guests, forming carbocation/carbenium ion intermediates,[1,4,7,8] are believed to play an important role in the acidic zeolites (HY and HZSM-5), but even so relatively few such transients have actually been identified.[1] Of interest here are possible *neutral* free radical intermediates in zeolites,[4,5,9] several examples of which have been reported from electron spin resonance (ESR) studies, but all from radiolysis or photolysis of specific organic precursors.[10−13] In analogy with carbocation intermediates and the importance of hydrogen exchange reactions,[8,14−16] one might expect that free radicals formed in situ by H-atom transfer from Brønstead-OH centers and addition to unsaturated bonds,[17] as proposed in some hydrocarbon-cracking mechanisms,[4,5] could also play a role in zeolite catalysis.

If neutral free radicals formed by H-atom addition are possible intermediates in zeolite catalysis, it is important to have techniques established with which they can be detected and their interactions determined. There have been ESR reports of H-adduct radicals formed from radiolysis studies of both olefinic and aromatic hydrocarbon guests in zeolites,[10,11] the ethyl ($CH_3\dot{C}H_2$) radical in particular being identified at low temperatures (90 K) in NaZSM-5.[11] However, little or no information on the nature of its binding sites or of its molecular interactions and motion within the zeolite framework was reported. There appear to have been no similar studies carried out in faujasites.

A hydrogen isotope of increasing importance as a spin probe of both the hyperfine interactions and molecular motions of free radicals is the positive muon (μ^+) and its muonium ($Mu = \mu^+e^-$) atom. The μ^+ is produced 100% spin polarized and this polarization can be effectively transferred to a free radical by Mu addition reactions, notably here by $Mu + C_2H_4 \rightarrow MuCH_2\dot{C}H_2$, giving the muon isotopic analogue[18−22] of the well-studied $CH_3\dot{C}H_2$ radical in the *bulk* phase.[23−27] The direct

* To whom correspondence should be directed: flem@triumf.ca.

† Based in part on the MSc. thesis of M. D. Bridges, Department of Chemistry, University of British Columbia. Present address: Graduate Studies, Department of Chemistry and Biochemistry, UCLA, Los Angeles, California 90095-1569.

‡ Alexander von Humboldt "wiedereinladung'', 2005, FU Berlin, and University of Stuttgart, Germany.

§ Present address: Department of Chemistry, Mount Allison University, Sackville, NB E4L 1G8, Canada.

10.1021/jp0686341 CCC: $37.00
Published on Web 06/14/2007

observation of muonium in different zeolites lends support to this Mu addition mechanism.[28,29] The muon spin polarization in a muoniated radical can be sensitively monitored by the μSR (muon spin relaxation or resonance) technique.[30,31] It has an important advantage over other magnetic resonance techniques in that essentially only *one* radical at a time is detected, thereby obviating concerns about radical−radical recombination reactions in the zeolite environment,[12] and, in addition, can be employed over a wide range of temperatures.

Though many Mu radicals have now been identified and characterized in bulk phases,[31−34] including the Mu−ethyl (MuC_2H_4) radical,[18−22] there have been relatively few such studies in the important catalytic environment of zeolites. Most μSR studies of this nature to date have focused on the Mu−cyclohexadienyl radical (MuC_6H_6), in faujasites[35,36] and in ZSM-5,[37,38] though some work on Mu−alkyl radicals in different zeolite frameworks[39] and also of the Mu−ethyl radical in silica powder,[40] of interest to the present study, has also been reported.

Of the many possible zeolite frameworks, the synthetic faujasites have large internal pore volumes with "supercages'' of ≈12 Å diameter, accessed by "windows'' ≈7.5 Å in diameter. There are eight of these supercages (sc) per unit cell, within which a variety of guest organic molecules can be accommodated, up to saturation loadings of five to six molecules/sc.[2,3,35,36,41] The present paper is the *first* study of the guest−host and hyperfine interactions of the *ethyl* radical in faujasites (NaY, USY, and HY), over a range of temperatures and loadings, by *any* technique. The emphasis here is on below-saturation loadings of one to three molecules/sc, which should exhibit high "sticking probabilities"[42] and which also faciliate the study of guest−host interactions at distinct adsorption sites, free from phase transitions and other cooperative phenomena that can occur at higher loadings.[3,41]

There are many possible binding sites for guest molecules in Y zeolites.[2,3,35,43−45] In NaY, ethene, like benzene, is expected to adsorb primarily at the S_{II} sites occupied by extraframework Na^+ cations within a supercage and/or at the window (W) sites between supercages. In HY/USY, exchanged protons form framework "onium'' charges with acidic −OH groups that serve as binding sites,[8,14,16,44,46] along with window sites.

There are a number of reasons for a μSR study of the Mu−ethyl radical in faujasites, apart from the fact that there appear to be no previous studies of the ethyl radical in these systems. First, there is only one structural isomer formed. Second, it has been well characterized in the liquid,[19,22] solid,[19] and gas,[18,20,21] as well as in silica powder,[40] the latter having the same basic SiO_2 framework structure as in zeolites. Third, and in contrast to MuC_6H_6,[35] when the Mu atom adds across the ethene double bond, there are *two* distinct proton hyperfine environments, the α protons at the $-CH_2^{\bullet}$ radical center and the β protons of the $-CH_2Mu$ group, providing additional means for characterizing the guest−host interactions of this key (H-atom) radical in the zeolite environment. Fourth, ethene itself has been studied by ab initio quantum methods in acidic zeolites,[16,47,48] and by inelastic neutron scattering, augmented by quantum Monte Carlo calculations in NaY,[43] which provide an important base for comparison of the sites and interactions of the Mu−ethyl radical. Fifth, quantum calculations of the hyperfine coupling constants and interactions of ethyl (and other alkyl) radicals in NaY and HY have recently been reported,[49] for which the present experimental data provide a valuable test.

2. Sample Preparation

Zeolite samples (NaY, HY, and USY) were obtained from Zeolyst International, with stated Si/Al ratios of 2.5 for NaY and HY and 15 for USY. These were loaded into stainless steel target cells and heated, under vacuum, in a tubular oven to drive off water of hydration. Since water can interact with both the framework oxygen atoms by hydrogen bonding[50] and with the cations in Y (and X) faujasites,[51] different temperature/time profiles for dehydration were carried out. In contrast to previous studies of the MuC_6H_6 radical in NaY,[35,36] the μSR results for MuC_2H_4 were more sensitive to heating procedures and off-line tests also revealed varying amounts of water loss depending on sample temperature and heating times. Some (HY/USY) samples were dehydrated at both lower (∼300 °C) and higher (∼500 °C) temperatures and for varying time periods. Those heated at lower temperatures gave unrealistic muon hyperfine couplings and are not considered further. Those (mainly USY) heated to the highest temperatures revealed much broader μSR line widths, likely due to the creation of paramagnetic defects, seen as well in the TF relaxation rates of Mu in different zeolite samples.[28] The data reported here are mostly for samples that were dehydrated at ∼400 °C overnight.

There was an important modification to the target cells described in ref 35. In that study the thin muon target entrance window (25 or 50 μm) was welded on after the cell had been filled with zeolite. New sample cells then required rewelding of the window. In the present study these cells were prefabricated, with threaded plugs on the sides of each cell to allow for easy changing of zeolite samples. Ethene was loaded from the gas phase, with pressure differences (∼50 Torr) measured from a known "standard volume'' (∼500 cm^3), to give loadings of between one and five ethenes/sc. Errors in pressure readings and weighings would nominally lead to loading errors ≲0.5 molecules/sc, but reproducibility effects, partly due to the temperature variations described above, could contribute to a larger overall level of uncertainty.

As in our previous study,[35] a given zeolite sample cell was mounted in a helium-flow cryostat for temperature control and was then placed in a superconducting magnet that provided magnetic fields up to 70 kG, aligned with the beam direction. Experiments were run on the M20 beam line at TRIUMF, which provides a spin-rotated muon beam, so that both longitudinal field (LF) and transverse field (TF) experiments could be run on the same sample. The spin-polarized surface muons passed through the target entrance window and stopped within the zeolite sample, forming the muoniated ethyl radical, by Mu addition to the olefinic bond.[21,28,29]

The temperature for all three samples was varied during the experiment in the range ∼5−320 K, and, for NaY (at 1/sc), up to 500 K, the latter for TF studies only. Temperature readings were monitored by two different thermocouples attached to the target cell, which typically gave consistent readings to better than a degree, which was also the level of reproducibilty found from off-line measurements of the temperature inside the cell. To check for possible effects of nonthermal equilibrium within the zeolite environment, as well as for reproducibility in the data, several runs were taken at alternating temperatures on both heating and cooling cycles, and over different run periods. No systematic effect was observed.

3. Experimental: Data Analysis and Results

Measurements of the hyperfine coupling constants (Hfc's) and interactions of the Mu−ethyl radical in NaY, HY, and USY were carried out over a range of loadings and temperatures. The utilization of spin-polarized surface muons and the μSR technique was identical to that described in ref 35. Reported are the muon and proton (α and β proton) Hfc's $A_\mu(T)$, $A_\alpha(T)$,

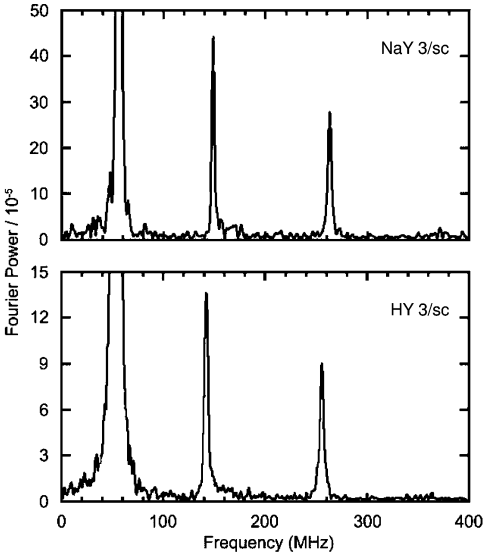

Figure 1. Representative FT-μSR spectra of Mu−ethyl in NaY (top) and HY (bottom) for a loading of 3/sc, at 180 K and a TF of 4.0 kG. The Fourier time window is 0.5 μs. The large (truncated) signal to the left is the diamagnetic signal (from unknown environments) at ν_D = 54.1 MHz. The other two signals are the two radical frequencies, ν_{R1} and ν_{R2} of eq 2, the sum of which gives the isotropic *muon* Hfc's, A_μ = 412 MHz for NaY (top) and 402 MHz for HY (bottom).

and $A_\beta(T)$, determined from both TF-μSR (for A_μ) and avoided level crossing resonance (ALC-μSR) measurements, along with the widths of these resonances, as well as the TF relaxation rates (λ).

3.1. TF and FT-μSR Spectra. In a TF experiment, the muon "asymmetry'' at the time of decay is given by

$$A(t) = \sum_i A_i e^{-\lambda_i t} \cos(\omega_i t + \phi_i) \qquad (1)$$

where A_i, λ_i, ω_i, and ϕ_i are the initial amplitude, relaxation rate, frequency, and initial phase for the ith environment. For the MuC_2H_4 radical, in TFs $\gtrsim$ 1.5 kG, there are three principal frequencies, one corresponding to diamagnetic muons (ν_D), and two radical frequencies, ν_{12} (=ν_{R1}) and ν_{43} (=ν_{R2}), that correspond to the allowed transitions of the spin Hamiltonian.[18,22,31,52] These can be clearly seen in Fourier transform (FT-μSR) spectra, revealing the characteristic radical precession frequencies[18,20,21,31,33]

$$\nu_{R_1} = |\nu_m - \frac{1}{2}A_\mu| \quad \text{and} \quad \nu_{R_2} = \nu_m + \frac{1}{2}A_\mu \qquad (2)$$

where A_μ is the *isotropic* muon−electron hyperfine Hfc and

$$\nu_m = \frac{1}{2}([A_\mu{}^2 + (\nu_e + \nu_D)^2]^{1/2} - \nu_e + \nu_D) \qquad (3)$$

with the Zeeman (Larmor) frequencies $\nu_D = \omega_\mu/2\pi = \gamma_\mu B$ for muons found in *diamagnetic* environments (γ_μ = 0.01355 MHz G^{-1}) and $\nu_e = \gamma_e B$ for the electron (γ_e = 2.8025 MHz G^{-1}). Examples of FT-μSR spectra in a TF of 4.0 kG are shown in Figure 1 for the MuC_2H_4 in NaY (top) and HY (bottom) at 180 K and for a loading of three ethenes/sc. The large (truncated) signal at ν_D = 54.1 MHz is due to muons in diamagnetic environments. The other two lines are the radical frequencies of eq 2. At this field, their sum gives directly the *muon* Hfc's, A_μ = 412 MHz in NaY and 402 MHz in HY. It is noteworthy that they are largely independent of zeolite framework.

The FT line shapes in Figure 1 are Lorentzian and the frequencies seen agree well with those found from fitting the time spectra, $A(t)$, from eq 1. Generally though, in polycrystalline environments, like zeolites, the Mu-radical precession frequencies can be modified by the angular dependence of the dipolar coupling, which can give rise to powder pattern spectral lines of asymmetric shape.[53] This can be seen in the FT spectra shown in Figure 2, for NaY at 3/sc, at different temperatures. (The spectrum at 180 K is the same as that in Figure 1, but transformed over a shorter time window.) At both lower ($\lesssim$150 K) and, surprisingly, higher ($\gtrsim$250 K) temperatures, the FT line shapes become noticeably broader and asymmetric, attributed to hyperfine anisotropy at the lower temperatures but indicative of additional framework interactions at the higher temperatures.

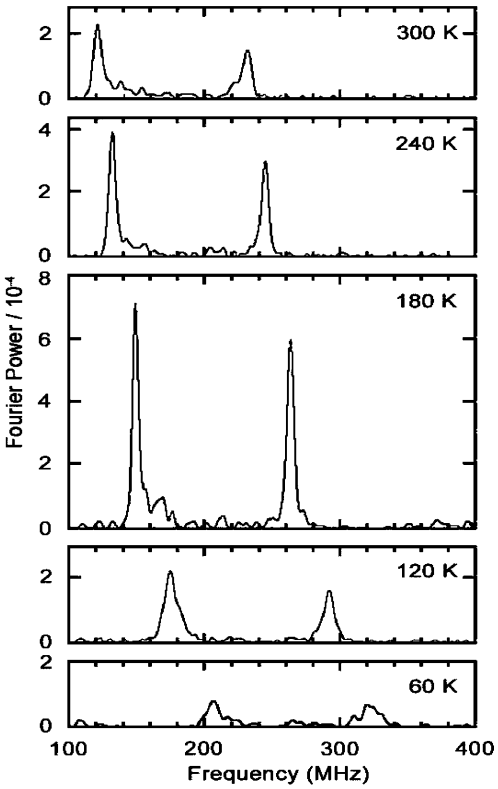

Figure 2. A comparison of FT spectra for the Mu−ethyl radical in NaY at a loading of 3/sc, at a fixed field of 4.0 kG, displaying just the two radical frequencies, ν_{R1} and ν_{R2}. The middle spectrum at 180 K is the same as in Figure 1 for NaY but transformed over a shorter time window of 0.25 μs. The FT lines broaden considerably and also become asymmetric at both lower and higher temperatures. Note also the increasing separation of the two radical frequencies with decreasing temperature, showing the T dependence in the muon Hfc, $A_\mu(T)$.

3.2. ALC-μSR Spectra. FT-μSR spectra give directly the *muon* Hfc's but may not be observable, due to excessive line-broadening effects, as commented above, or slow radical formation, which guarantees dephasing in high TFs. In these cases, the muon Hfc may be found by the ALC-μSR technique, in high LFs, which also provides measurement of the *nuclear* Hfc's, A_k.[31,33,35,36,54] An ALC signal appears as a "dip'' in the time-integrated decay asymmetry one corresponding to a resonant transfer of muon spin polarization from the backward to the forward direction as the magnetic field is scanned.[35,54] Typically, several sweeps of the longitudinal field range were carried out, in alternating directions, incremented in steps of about 100 G, depending on conditions.

There are three specific types of ALC resonances corresponding to magnetic selection rules and which reflect different aspects of the spin Hamiltonian.[18,31,35,54] The Δ_0 resonance represents a "flip-flop'' exchange of spin polarization between the muon and a nuclear (here proton) spin. It is driven

(indirectly) by matrix elements that involve the operators $\mathbf{S}^{\mathbf{e}}_{-}\mathbf{I}^{\mu}_{+}$ and $\mathbf{S}^{\mathbf{e}}_{+}\mathbf{I}^{\mathbf{p}}_{-}$, arising mainly from the *isotropic* hyperfine interaction, from which the proton Hfc, A_p, is determined. Similar contributions can also arise from the *anisotropic* interaction, in crystalline environments, in which case the *effective* proton Hfc depends on the angles of the hyperfine tensor between the proton spin and the direction of the applied field, $\tilde{A}_p = A_p(\theta,\phi)$. A Δ_0 resonance is the only one seen in gases or liquids or in any environment where dipolar couplings are averaged out by fast rotational motion.[55−58]

The Δ_1 resonance is a pure muon spin-flip and is induced directly through the coupling of Zeeman states from the *anisotropic* part of the muon−electron hyperfine interaction, via matrix elements of the operators $\mathbf{S}^{\mathbf{e}}_{\mathbf{z}}\mathbf{I}^{\mu}_{+}$. It is then always dependent on the angles between the muon spin and the field direction, via the effective muon Hfc, $\tilde{A}_\mu = A_\mu(\theta,\phi)$. Since the muon hyperfine tensor has a fixed orientation on the radical and is observable only in anisotropic environments, the Δ_1 resonance provides a sensitive means to study reorientation dynamics of that radical. As previewed above, A_μ can also be found from a TF experiment (e.g., Figure 1), where a muon spin-flip arises from transitions due to the $\mathbf{I}^{\mu}_{+}$ operator, a correspondence that provides a valuable identification of a Δ_1 line in ALC-μSR spectra. A further Δ_2 ALC "flip−flip'' transition is always much weaker and is of no consequence here.

In a *single crystal*, the ALC line shapes are Lorentzian and the positions of each resonance will be at a magnetic field (B_r) that is dependent on the angles characterizing the effective hyperfine coupling constants, $\tilde{A}_\mu$ and $\tilde{A}_p$, for the Δ_1 and Δ_0 resonances, respectively.[54,59] In the *polycrystalline* environment of a zeolite, the superposition of these different resonant fields leads to a powder pattern which, for a *static* MuC_6H_6 radical, gives a *symmetric*, albeit non-Lorentzian, line shape.[35,37,54,59] In previous studies of the Mu−cyclohexadienyl radical in NaY,[35] such symmetric line shapes were seen for both the Δ_1 and Δ_0 resonances, over a wide temperature range. These were fit to Gaussians, from which the muon (A_μ) and proton (A_p) Hfc's were determined from the positions of the minima and eqs 4 and 5

$$B_r(\Delta_1) = \frac{1}{2}\left|\frac{A_\mu}{\gamma_\mu} - \frac{A_\mu}{\gamma_e}\right| \tag{4}$$

$$B_r(\Delta_0) = \frac{1}{2}\left|\frac{A_\mu - A_p}{\gamma_\mu - \gamma_p} - \frac{A_\mu + A_p}{\gamma_e}\right| \tag{5}$$

respectively, with the gyromagnetic ratio $\gamma_p = \gamma_\mu/3.184$. The same assumption is made here for the MuC_2H_4 radical and is justified further below. It is worth noting from eq 5 that, in contrast to ESR,[60] the ALC-μSR technique is sensitive to the *sign* as well as the magnitude of the nuclear Hfc's. (Equation 5 is actually a slight approximation in that small differences in resonance positions due to equivalent protons have been ignored. However, these shifts are at the 0.3% level,[61] well within the width of each resonance.)

Figures 3 and 4 show background-corrected (see ref 35) ALC-μSR spectra at a loading of 1/sc for the Δ_1 resonances of the Mu−ethyl radical at different temperatures in NaY and HY, respectively, up to the highest temperatures at which these are observed. The solid lines in each case are Gaussian fits to the data, consistent with the broad, symmetric nature of each Δ_1 resonance seen, as outlined above. At temperatures near 200 K

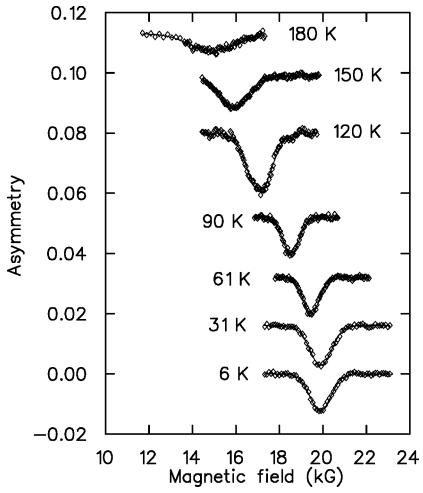

Figure 3. Background-corrected ALC-μSR spectra for the Δ_1 resonances of the Mu−ethyl radical in NaY at a loading of 1/sc, over a range of temperatures. The symmetric line shapes seen are well accounted for by the phenomonological Gaussian fits shown (solid lines). Note the relatively constant line widths up to 120 K, but which broaden noticeably at somewhat higher temperatures and could not be observed above 180 K.

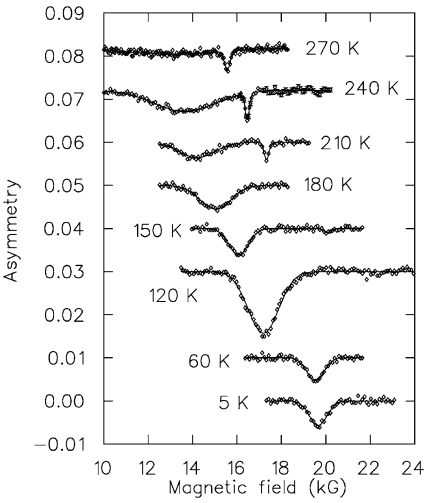

Figure 4. Background-corrected ALC-μSR spectra at different temperatures for the Δ_1 resonances of the Mu−ethyl radical in HY at a loading of 1/sc. See caption to Figure 3. Though highly broadened, these could (just) be observed up to 270 K in HY, somewhat higher than those in NaY, but then again disappear into the baseline. The much sharper, higher field, lines seen at 210, 240, and 270 K are the Δ_0 level crossings for the β protons. Solid lines are Gaussian fits to the data in all cases.

the Δ_1 lines become too broad to fit and their widths were determined from line positions fixed at the fields expected from TF measurements of the muon Hfc's, A_μ. In Figure 4 the much sharper higher-field resonances seen at temperatures of 210, 240, and 270 K are the Δ_0 lines for the β protons of the Mu−ethyl radical in HY. Figure 5 plots these resonances for both the β (lower fields) and α (upper fields) protons in NaY. In these cases the solid lines are fits to a Lorentzian line shape. Note how narrow the Δ_0 lines tend to be in comparison with the Δ_1 resonances (Figure 4), though broadening is again seen at the highest temperatures for the α resonances in NaY (Figure 5).

3.3 Comparative Plots of $A_\mu(T)$ and $A_p(T)$. Similar-looking ALC-μSR spectra as seen in Figures 3−5 were obtained in USY at a loading of 1/sc and in HY at a loading of 5/sc, and as well, TF data (only) were taken for NaY and HY at a loading of

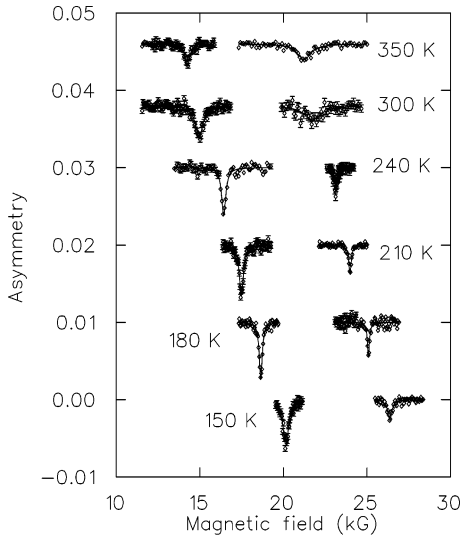

Figure 5. Background-corrected level crossings at different temperatures for the β (lower fields) and α (upper fields) proton Δ_0 resonances of the Mu−ethyl radical in NaY at a loading of 1 ethene/sc. The solid lines shown are Lorentzian fits to the data. The positions of the minima shown give the proton coupling constants from eq 5, in concert with a known value for A_μ. The widths are fairly constant with increasing temperature, except for the α resonance, which broadens noticeably at the highest temperatures.

3/sc. The ALC data showed little or no change in resonance positions for either Gaussian or Lorentzian fits. For the TF data, time-differential fits to time-domain spectra, $A(t)$, were in good agreement with the FT results, with a minimum combined error of ± 1 MHz for A_μ. At the lower temperatures, the TF lines become too broad and asymmetric to give reliable fits (see Figure 2), so in these cases A_μ was found from the centroid positions of the Δ_1 resonances and eq 4, with errors that typically exceed 1 MHz. The proton Hfc's were similarly determined from the positions of the Δ_0 resonances, with generally larger errors than those for A_μ, as expected from eq 5.

The results of the analysis for all three frameworks, for a loading of 1/sc, are given in Tables 1, 2 and 3, respectively. For the Δ_1 resonances, it is the "2σ'' widths from the Gaussian fits that are recorded (the full width at half-maximum (fwhm) is 2.35σ), whereas for both the β and α proton Δ_0 resonances, the fwhm from the Lorentzian fits are recorded. For the Hfc's, the overall errors shown reflect both statistical and systematic errors, the latter estimated from the level of reproducibility found from different determinations. The errors shown for the widths are from fits to the level crossing resonances only and reflect as well a similar estimate of systematic uncertainty. The trends in the widths to increase with increasing temperature are similar for NaY and HY, but this is less clear in USY (Table 3), where the line widths are broader at lower temperatures and remain more constant with increasing temperature, though enhanced broadening is also seen at the highest temperature (320 K). Much of these data, however, were obtained from samples that had been subjected to higher-temperature preparation, and thus exhibited artificially enhanced widths, as commented on earlier. Even so, reliable Hfc's could still be determined, but with typically larger errors (Table 3).

The data for the *muon* Hfc's of MuC_2H_4 in NaY, HY, and USY, from the entries in Tables 1−3 as well as results from other loadings, are plotted vs temperature in Figures 6−8. In Figures 7 and 8 (and Figure 11 later) these are plotted in "reduced units'', $A_\mu' = A_\mu \gamma_p/\gamma_\mu = A_\mu/3.184$, in order to correct for the trivial mass difference between proton and muon gyromagnetic ratios, and which facilitates comparison with similar μSR data reported elsewhere in the bulk,[19,20,22] also plotted in Figures 7 and 8 (crosses and dashed lines) and on silica powder.[40] Given an expected loading uncertainty of ~0.5/sc, only small changes in muon Hfc's are seen for different frameworks and for different loadings, though there does seem to be a slight dependence on loading for the HY data (Figure 8), where the values of $A_\mu'(T)$ at 5/sc [HY(5)] are some 10% below those for HY(1) and closer to bulk values. The lines drawn in all these figures are guide lines only, intended to show the trends in the data.

The data for the *proton* Hfc's, from fits to the Δ_0 resonances (e.g., Figure 5), are similarly plotted for the β protons, $A_\beta(T)$, and α protons, $A_\alpha(T)$, in Figures 9 and 10, respectively. In Figure 10, the proton Hfc's determined from ESR measurements of the ethyl radical[24−26] are also plotted (vertical crosses and dash-dot-dot line). As with the muon Hfc's in Figures 7 and 8, the trends are similar in the β proton Hfc's in all three frameworks and in the bulk, though with the expected opposite dependence, increasing with increasing temperature. In contrast, the T dependence of the α proton Hfc's (Figure 10) show rather marked departures from the bulk μSR and the ESR data, particularly at lower temperatures. Not plotted are the results for USY (Table 3), which lie quite close to the HY data.

4. Discussion and Comparison with Theory

4.1. Binding Sites and Peak Assignments. The Mu atom adding to the ethene double bond places the muon in the β position, with the unpaired electron then in a p_z orbital on the α carbon, giving two distinct Δ_0 resonances for β and α protons in addition to the Δ_1 muon resonance. From eq 5, the α proton resonance, with a negative Hfc,[23,27,60] will always lie above that for the β protons, with the muon resonance falling at the lowest field, the order seen in the ALC-μSR plots of Figures 3, 4, and 5 (and similarly so for USY). The *positions* of these resonances tell us about site locations while the *widths* tell us about molecular dynamics.

In NaY there are four equivalent S_{II} sites occupied by Na^+ within a supercage,[3,45,62] as well as two equivalent window sites between supercages, nominally providing six possible binding sites for benzene[3,35,46,62] or ethene.[43] From Figures 7 and 8, at the lowest temperatures, in the region of the "McConnell plateau'', the reduced muon Hfc's, A_μ', are about 10% higher than those seen in the bulk and slightly dependent on loading in HY. Though only half of the ~20% shifts seen earlier for the MuC_6H_6 radical in NaY,[35,36] these are still much larger than the ~2% shifts seen for MuC_2H_4 in silica powder,[40] and, as for MuC_6H_6, are taken as evidence for binding of the Mu−ethyl radical to cations at S_{II} sites in NaY, in accord with recent calculations of the binding energy (BE) of the ethyl radical to these sites.[49]

These calculations assume a "T-atom'' model for C_2H_5·NaY, where the cation is centered at the S_{II} site at an optimized distance of 2.6 Å above an O-linked six-membered ring of tetrahedral (T) Si atoms that contribute to the boundary of each supercage. The charge imbalance introduced by the Na^+ is uniformly compensated by a countercharge on each of the silicon T-atom sites. Density functional theory (DFT) gives a BE of 137 kJ/mol (uncorrected for zero-point energy) for the ethyl radical at the cation site in NaY. This seems to be a surprisingly large value though in comparison both with the DFT calculations of the binding of the MuC_6H_6 radical in a NaY cluster by Macrae and Webster, of ~40 kJ/mol,[63] and in comparison with the BE of ethene itself to Na^+ in NaY, also ~40 kJ/mol in ref

TABLE 1: Muon and Proton Hfc's and ALC Widths for MuC_2H_4 in NaY(1/sc)

	muon Hfc's[a]		β-proton Hfc's[b]		α-proton Hfc's[b]	
T (K)	A_μ (MHz)	width (G)[c]	A_β (MHz)	fwhm (G)[d]	A_α (MHz)	fwhm (G)[d]
6	542(2)	1000(50)				
31	543(2)	1000(50)				
61	530(1)	750(50)				
90	505(2)	750(50)				
120	465(2)	1200(100)	59(3)			
140[e]	440(1)	TF only				
150	434(2)	1400(100)	58(3)	490(160)	−58(3)	360(80)
160[e]	422(1)	TF only				
180	406(1)	2100(300)[f]	57.3(1.3)	260(30)	−62.0(1.5)	170(30)
210	387[g]	not scanned	60(2)[g]	350(40)	−60(2)[g]	220(30)
220[e]	380(1)	TF only				
240	371[g]	1600(300)	63(2)[g]	350(40)	−60(2)[g]	220(40)
270	358(1)	∼2500[f]	65.0(1.0)	380(60)	−60.5(1.5)	900(200)[h]
300	349(1)	not fitable	68.5(1.0)	600(100)	−59(3)	900(200)[h]
320	343(2)	∼3000[f]	69(2)	450(120)	−60(3)	1200(100)[h]
350	336(2)	not fitable	70(2)	450(100)	−60(2)	1100(300)[h]

[a] Where possible, determined from both TF and ALC data, with averaged values reported. At low temperatures, ≲150 K, mainly determined from the positions of Gaussian fits to the Δ_1 resonances and eq 4. See Figure 3. At higher temperatures, mainly found from TF data and eq 2. See Figure 1. Systematic errors also included, determined from reproducibility measurements. [b] β proton and α proton Hfc's, A_β and A_α, determined from the positions of Lorentzian fits to the Δ_0 resonances and eq 5. See, e.g., Figure 5. Errors depend on the positions of both the Δ_1 and Δ_0 resonances and thus are greater than or equal to those given for A_μ and include an estimate of systematic errors as well. [c] The widths (in gauss) of the Δ_1 (muon) resonances are "2σ" widths (fwhm = 2.35σ) from Gaussian fits to the data, as in Figure 3. [d] The widths (in gauss) for the Δ_0 (proton) resonances are the fwhm values from Lorentzian fits to the data, as in Figure 5. [e] No ALC scans, A_μ determined from TF data only. [f] The position of the broad Δ_1 resonance was fixed at the value determined from the TF result. [g] The muon Hfc's not measured, or poorly determined, so estimated from trends for the purpose of determining the value of A_p. Errors on the latter taken to be ±2 MHz. [h] Widths of the α proton Δ_0 resonances noticeably much broader at these temperatures, ≈1000 G, and were difficult to fit, often near the end of the scan range.

TABLE 2: Muon and Proton Hfc's and ALC Widths for MuC_2H_4 in HY (1/sc)

	muon Hfc's[a]		β-proton Hfc's[b]		α-proton Hfc's[b]	
T (K)	A_μ (MHz)	width (G)[c]	A_β (MHz)	fwhm (G)[d]	A_α (MHz)	fwhm (G)[d]
5	535(2)	800(70)				
30	530(4)[e]	≈1500[e]				
60	532(2)	800(70)				
120	468(2)	1300(100)				
150	439(2)	1100(100)	63(2)	600(200)		
180[f]	409(1)	1600(300)	63.5(1.5)	600(200)	−52.8(1.5)	350(150)
210[f]	387(1)	1500(300)	64.0(1.5)	340(50)	−55.0(1.5)	350(80)
240[f]	372(1)	2800(600)	66.0(1.5)	350(60)	−55.0(1.5)	200(50)
270[f]	357(1)	≳3000	67.3(1.5)	350(60)	−56.5(1.5)	300 (50)
298[f]	348(1)	not fitable	67.9(1.2)	250(30)	−58.5(1.2)	300(50)
300[f]	346(1)	3500(500)	68.8(1.5)	260(60)	−57.3(1.5)	600(200)
322[f]	340(1)	not fitable	69.0(1.2)	550(80)	−57.5(1.2)	400(80)
350[f]	333(1)	not fitable	70.0(1.5)	480(40)	−57.6(1.5)	300(100)

[a] See Figure 4 and notes to Table 1. No higher temperature data points beyond 350 K. [b] β proton and α proton Hfc's from Δ_0 resonances. See Figure 4 (for β proton) and notes to Table 1. [c] See Figure 4 and notes to Table 1. [d] See Figure 4 (for β proton) and notes to Table 1. [e] From high-temperature sample preparation (≳450 °C), giving a larger error and an unreliable ALC line width. [f] For temperatures ≥180 K, the muon Hfc's, A_μ, mainly found from TF data. In many cases the position of the Δ_1 resonance was determined (and fixed) from the TF result. Very broad ALC lines at the higher temperatures (Figure 4) that often could not be fit.

49, consistent with other calculations of ethene binding in zeolite environments,[43,47,48] and with experimental determinations of heats of adsorption. One would not a priori expect such a large change in BE for the radical, which is indeed the case for benzene and Mu−cyclohexadienyl in NaY.[63]

However, both bond conjugation in the benzene system as well as differences in basis sets, cluster sizes, and methodology[43,44,63,64] will certainly play a role here. The calculations of Macrae and Webster for the binding energy of MuC_6H_6 in NaY are based on local changes in energy, whereas those of Ghandi et al. for MuC_2H_4 are based on the energy difference of the molecule from infinity to a global equilibrium geometry, which could well lead to large differences in calculated binding energies. Still, it is interesting to note further that both Macrae and Webster and Ghandi et al. also compare calculations for binding to a bare Na^+ with the NaY environment, finding completely opposite behavior: for benzene and Mu−cyclohexadienyl, both the benzene and the radical give a marked increase in BE, to ∼100 kJ/mol[63] whereas for the Mu−ethyl radical a marked decrease of a similar magnitude is seen, to ∼63.5 kJ/mol.[49] What is clearly needed here is a self-consistent comparison of the BEs of both the MuC_6H_6 and MuC_2H_4 radicals in the same environments.

Though the difference noted above in shifts of the muon Hfc's for the MuC_6H_6 and MuC_2H_4 radicals in NaY is significant, the most dramatic difference is simply in the number of ALC resonances seen. For MuC_6H_6, *six* resonances are observed, depending on temperature and loading, three clear Δ_1 lines and three (weaker) Δ_0 lines,[35,36] whereas for MuC_2H_4 only *three* in total are seen (in all three frameworks), a Δ_1 and the two Δ_0 resonances for the α and β protons. This is also the case in the bulk solid[19] and in silica powder,[40] meaning that there can only

TABLE 3: Muon and Proton Hfc's and ALC Widths for MuC_2H_4 in USY (1/sc)

	muon Hfc's[a]		β-proton Hfc's[b]		α-proton Hfc's[b]	
T (K)	A_μ (MHz)	width (G)[c]	A_β (MHz)	fwhm (G)[d]	A_α (MHz)	fwhm (G)[d]
5	530(3)	1600(200)				
30	534(2)	1400(100)				
45	528(2)	1300(200)				
90	492(3)	1800(200)				
105	488(5)[e]	1600(100)				
120	473(4)[e]	1000(200)				
150	421(5)[e]	1400(200)				
180[f]	389(3)	1100(200)				
195[f]	388(4)[e]	1200(200)				
210[f]	374(4)[e]	1600(200)	64(3)	450(50)	−58(3)	360(60)
240[f]	364(2)	1800(300)	66(3)	420(80)	−57(3)	250(50)
270[f]	348(2)	not scanned	67(2)	380(50)	−59(2)	400(100)
285[f]	346(2)	not scanned	67(2)	300(40)	−58(2)	250(50)
300[f]	340(1)	not scanned	68(2)	500(60)	−59(3)	300(100)
320[f]	334(1)	≈ 3000	68(1)	500(150)	−60(1)	400(100)

[a] See notes to Table 1. No higher temperature data points beyond 320 K. [b] β-proton and α-proton Hfc's. See notes to Table 1. [c] See notes to Table 1. The Δ_1 ALC line widths are generally broader than in HY and change less with increasing temperature, attributed to higher sample preparation temperatures (see note *e*). [d] See note in Table 1. [e] Determined from a combination of data, including some from high-temperature sample preparations. In general, ALC widths are less reliable for these data than for the NaY and HY data. See notes to Table 2. [f] The muon Hfc's, A_μ, found from TF data only. In most cases this was fixed in fitting the Δ_1 ALC data, in order to determine the line width. See notes to Tables 1 and 2.

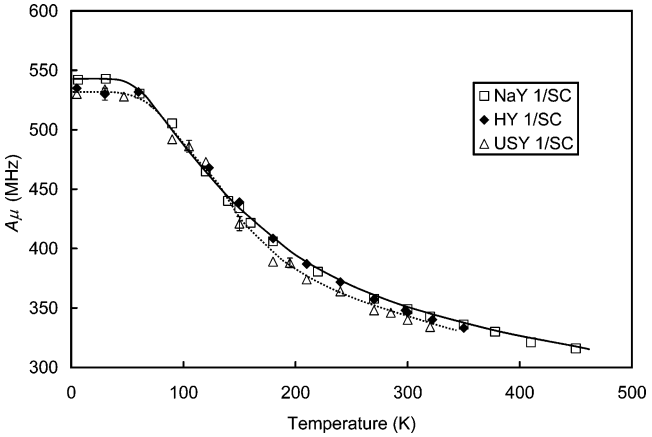

Figure 6. The cation dependence at a loading of 1/sc for the muon Hfc's vs temperature, $A_\mu(T)$, for the Mu−ethyl radical in NaY, HY, and USY. The plotted values are taken from Tables 1 to 3 and reflect combinations of TF-μSR and ALC-μSR, as explained in the text. The points shown are typically larger than the error bars. The USY data (dotted line) tend to fall below the NaY and HY data (solid line), but the effect is slight, demonstrating little or no framework dependence.

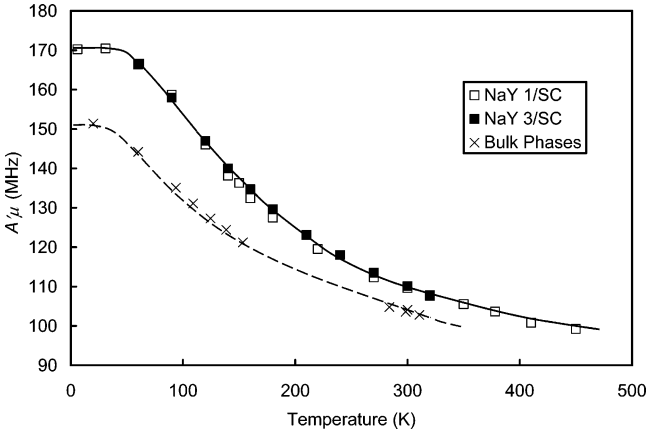

Figure 7. The loading dependence of the muon Hfc's vs temperature, in "reduced units", $A_\mu'(T) = A_\mu(T)/3.184$, at 1/sc and 3/sc for the Mu−ethyl radical in NaY (solid line) compared with similar data obtained in the bulk (dashed line).[19,20] The 3/sc NaY points were all determined from TF-μSR data only. The 1/sc points are the same as those plotted in Figure 6. The lines are guides to the trends only. Note the enhanced muon Hfc's compared to (extrapolated) bulk values at the lowest temperatures.

be a *single* binding site for Mu−ethyl, believed to be the S_{II} cation site in NaY, supported as well by the calculations of ref 49.

The binding sites in HY are more complex than those seen in NaY. There are four crystallographically distinct O atoms that H^+ cations could bind to, forming bridging OH groups,[14] but only two of these, the so-called O1H and O4H sites (there does not appear to be uniformity of notation[46]) point toward the SC and thus could accommodate ethene[44,48,49] or benzene.[46] Here a T-atom model is not appropriate, since the −OH groups are part of the framework and are not ring centered, with specific site locations for Al required as well. From the DFT calculations of ref 49 for the ethyl radical in HY, very large binding energies are reported: 242 kJ mol^{-1} at the O1H site and 327 kJ mol^{-1} at the O4H site, the latter at an optimum distance of 1.09 Å (about half that in NaY). Such a large difference in BEs implies that there could be two distinct binding sites for the Mu−ethyl radical in HY, but as in NaY, only a single site is seen, likely the O4H site, on thermodynamic grounds. There is evidence for benzene binding to only a single site in HY as well.[46]

Somewhat surprisingly, there is no evidence from the present study for MuC_2H_4 bound at window sites between supercages, even at higher loadings (5/sc in HY), which is expected for ethene[43] and clearly seen in the Δ_1 resonances for the MuC_6H_6 radical bound to these sites in NaY.[35,36] Benzene though is better matched to the W-site geometry and as well has a stronger propensity for H-bonding with the 12-atom ring of oxygens.[3,35]

4.2. Temperature Dependence of the Muon Hfc's, $A_\mu'(T)$. As is well-known, measurements of hyperfine coupling constants in free radicals determine the electron spin density on nuclei and depend on geometric structure, spin polarization, and hyperconjugation.[23,27,49,65,66] Effects of this nature would be expected to be strongly modified for free radicals interacting with cation sites in zeolites, compared to the bulk, and which accordingly could provide a guide to the role played by free radicals as intermediates in these important catalytic environments.

The equilibrium geometry of the unperturbed (and unsubstituted) ethyl radical ($CH_3\dot{C}H_2$) consists of a largely tetrahedrally bonded CH_3 group at the β carbon and an sp^2 bonded CH_2 group

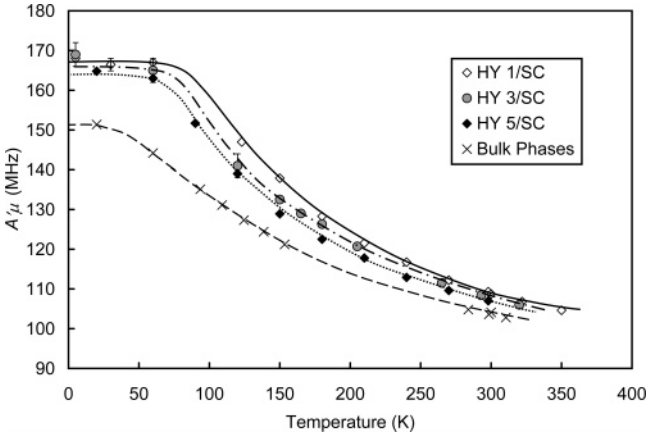

Figure 8. The temperature and loading dependence of $A_\mu'(T)$ for the Mu−ethyl radical in HY at loadings of 1/sc (solid line), 3/sc (dash-dot line), and 5/sc (dotted line), compared with similar data from the bulk. See caption to Figure 7. There is an indication of some loading dependence outside the level of natural scatter, with the HY(5) data falling closer to that of the bulk.

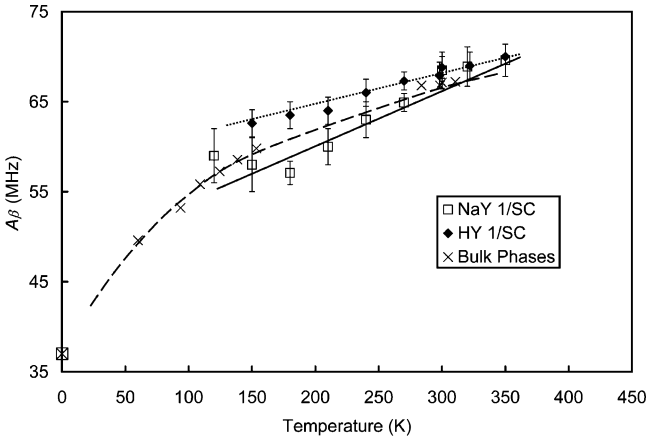

Figure 9. The cation dependence at a loading of 1/sc for the β *proton* Hfc's of the Mu−ethyl radical vs temperature in NaY (solid line) and HY (dotted line) compared with similar data obtained in the bulk (crosses and dashed line).[19] The lines are again guides to the trends only. Similar data for USY tends to fall midway between those for NaY and HY. A limited amount of data for the β proton Hfc's in HY-(5) are similar to the trend shown for HY(1). The bulk μSR data tend toward the calculated value of 37 MHz at 0 K for the MuC_2H_4 radical (in vacuum), from Ghandi et al.,[49] and the same line could well accommodate the NaY data, tending then toward the calculated value of 37.5 MHz in NaY (open square with cross).

at the α carbon, with an expected planar geometry,[22,60] but which exhibits large amplitude out-of-plane motion.[23,27] The basic geometry remains the same upon Mu substitution ($MuCH_2\dot{C}H_2$), but the lighter (Mu) isotope favors the conformation where the unpaired electron in the p_z orbital is parallel to the C−Mu bond at the β carbon.

Assuming a planar geometry at the C_α position (angle $\phi = 0$), the temperature dependence of the β muon Hfc's are expected to follow the well-known "McConnell relation",[19,20,22,60]

$$A_\mu' = L + M\langle\cos^2\theta\rangle \qquad (6)$$

where θ (measured relative to its equilibrium value) is the dihedral angle between the axis of the p_z orbital and the C_β−X bond for atom "X" = H, D, or Mu. Hyperconjugation effects (delocalization of the spin density) depend on geometry and are largely reflected in the value of M whereas the L parameter

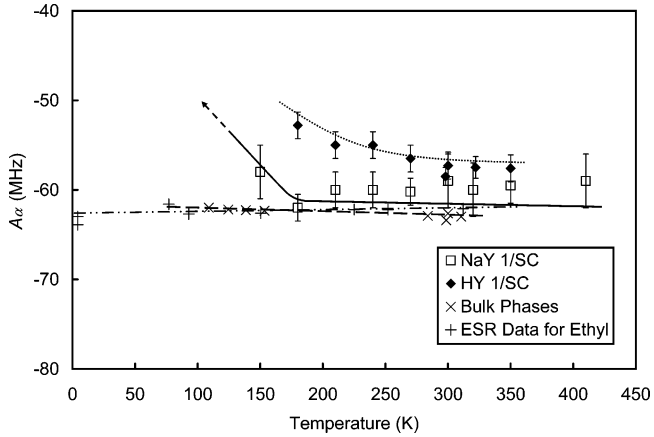

Figure 10. The cation dependence at 1/sc for the α *proton* Hfc's of the Mu−ethyl radical vs temperature in NaY and HY. See caption to Figure 9. The guide lines exhibit the same upward trend at the lower temperatures for the HY (dotted line) and NaY (solid line), the latter predicated on the calculations of ref 49 at 0 K in NaY (−33 MHz, indicated by the arrow). This trend at the lower temperatures in both NaY and HY stands in contrast to that for both the bulk μSR data (crosses and dashed line) and the ESR data for the ethyl radical (vertical crosses and dash-dot-dot line), the latter even appearing to exhibit a slightly positive slope.

is primarily a measure of spin polarization ($L \ll M$). The observed value of $A_\mu'(T)$ is a Boltzmann-weighted average over different conformations that depend on the torsional barrier to internal rotation about the C−C bond.[19,22,49,65,66] Within the Born−Oppenheimer approximation, this barrier arises primarily from differences in zero-point energy (ZPE) contributions to the total energy, between the minimum and maximum energy conformations for alignment with the p_z orbital.

For the unsubstituted ethyl radical, due to the C_3 symmetry of the CH_3 group, this barrier is small, $\lesssim$200 J/mol,[27,65] consistent with observations of essentially no T dependence for ESR-measured proton Hfc's of the ethyl radical[25,26] (see Figure 13 below). In contrast, for X = Mu, the experimentally determined barrier for bulk ethene, between the energy of the eclipsed ($\theta = 0°$) and staggered ($\theta = 90°$) conformations is ∼2800 J/mol,[19,22] due mainly to the huge ZPE shifts of the C−Mu stretch.[65,66] Such a large barrier dictates that the eclipsed C−Mu bond is the minimum energy conformation, giving favorable hyperconjugative orbital overlap and maximum muon Hfc's near 0 K. With increasing temperature, the C−Mu bond rotates away from this favored orientation, toward the plane of the $-CH_2$ group, thereby decreasing the muon Hfc (and concomitantly increasing the β proton Hfc's). These qualitative features are clearly seen in the $A_\mu'(T)$ data for the MuC_2H_4 radical in NaY and HY in Figures 7 and 8, the first time such a dependence has been reported in zeolites. It is somewhat surprising though that the overall T dependence of A_μ', for Mu−ethyl interacting with zeolite sites, is so similar to that in the bulk (dashed lines).

This similarity can be placed in context by comparing the values of the McConnell parameters L and M of eq 6, determined from fitted contributions of Boltzmann-weighted conformers to the experimental temperature dependences of the muon Hfc's in the bulk. Ramos et al.[22] and Yu[19] (who included the higher temperature gas-phase data of ref 20), report $L \sim -15(\pm3)$ MHz and $M \sim 190(\pm10)$ MHz, depending on assumptions. At high enough temperatures, in the limit of free rotation, $A_\mu'(\infty) = L + 1/2M$, and from this value and that near 0 K, $A_\mu'(0) = L + M$, one can qualitatively estimate the values of the McConnell parameters for the data in Figures 7 and 8. From the fitted

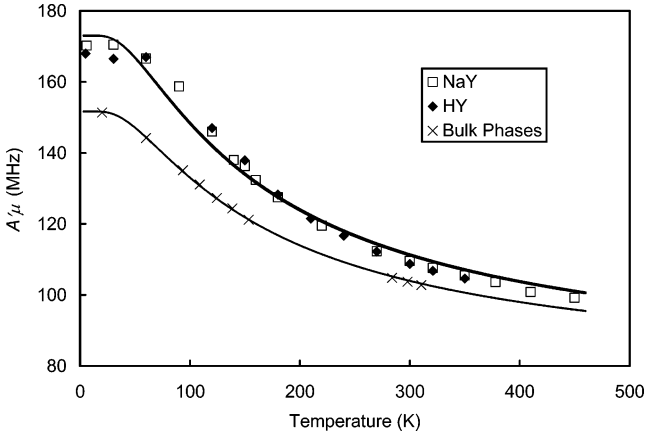

Figure 11. Fit of eq 7 to the temperature dependence of the reduced muon Hfc, A_μ', for MuC_2H_4 in NaY and HY at a loading of 1/sc (Figure 6) and in the bulk. Though both the NaY and HY data are plotted together, they are fitted separately, but the fitted lines are essentially indistinguishable (thick upper line). The fitted activation energies for torsional motion are $E_{ROT} = 1155 \pm 25$ J mol^{-1} (NaY), $E_{ROT} = 1140 \pm 40$ J mol^{-1} (HY), and $E_{ROT} = 1176 \pm 16$ J mol^{-1} (in bulk).

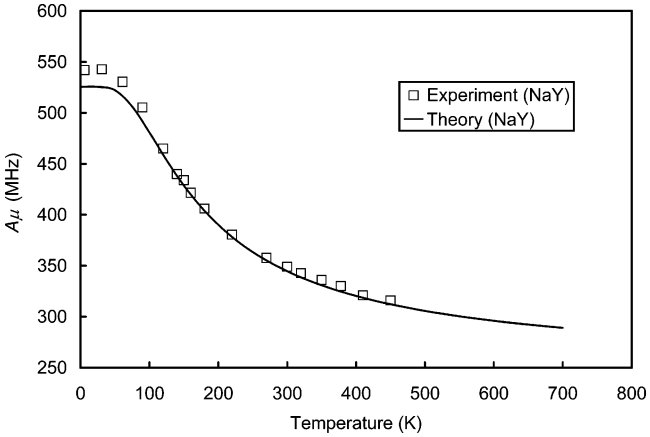

Figure 12. Theoretical values for the T dependence of the isotropic muon Hfc's, $A_\mu(T)$, for the Mu−ethyl radical in NaY at 1/sc, from the "T-atom'' model and DFT calculations of ref 49, compared with the experimental results (open squares). The calculated theory points have been connected with a smooth curve (solid line).

parameters in the bulk, $A_\mu'(\infty) \sim 80$ MHz, which can be compared with the (temperature-independent) ESR value for CH_3 group rotation of 75.3 MHz.[25,26] This difference of about 5 MHz may represent a real "residual isotope effect'',[20] but it may also be the case, for temperatures well above rotational barrier heights, that $A_\mu'(\infty)$ is isotope independent and hence given by the ESR value of 75.3 MHZ. Adopting this view here gives $L \sim -20$ MHz and $M \sim 190$ MHz for NaY, independent of loading, and for HY(1), $L \sim -18$ MHz and $M \sim 186$ MHz, while for HY(5), $L \sim -13$ MHz and $M \sim 176$ MHz, all comparable to the fitted values in the bulk.

Alternatively, one can treat the T-dependence of $A_\mu'(T)$ by a classical Arrhenius form, written as[32]

$$A_\mu'(T) = A_\mu'(\infty) + [A_\mu'(0) - A_\mu'(\infty)](1 - e^{-E_{ROT}/RT}) \quad (7)$$

where E_{ROT} is the activation energy for C−C bond rotation. A fit of this expression to the temperature dependence of Mu−ethyl in NaY and HY, at a loading of 1/sc, as well as to the data previously reported in the bulk,[19,20] is shown in Figure 11. In these fits $A_\mu'(\infty) = 75.3$ MHz. Assuming 80 MHz for this free rotation limit, in accord with the residual isotope effect mentioned above, gave consistently worse fits to the data. The fit to the bulk data in Figure 11 is excellent (lower solid line) and yields an activation energy, $E_{ROT} = 1176 \pm 16$ J/mol, the same as that reported by Roduner et al.,[32] over the more restricted temperature range of the liquid phase. The results for the NaY and HY data in Figure 11 are not so good (the fits overlap and appear as one thick solid line), particularly around 100 K. The trend though and the higher temperature data are well reproduced, giving $E_{ROT} = 1155 \pm 25$ J/mol in NaY and 1140 ± 40 J/mol in HY, essentially the same as in the bulk. That relatively poor fits are found in the zeolite environment is not surprising, given the simplified function of eq 7. There is likely some coupling between C−C bond rotation and motion of the Mu−ethyl radical as a whole at its binding site, that is not accounted for.

Though one might have expected higher activation energies for C−C bond rotation of the Mu−ethyl radical in the zeolite environment, compared to the bulk, even from this simple model, that they are the same is consistent with the similarity noted earlier in McConnell parameters, both results suggesting that the ethyl radical maintains a fairly unrestricted geometry in its binding to faujasite sites. This implies in turn that the radical is tilted well away from the plane of atoms containing the Na^+ ions in NaY and −OH sites in HY, which finds favor with the calculated geometries of Ghandi et al.,[49] where the ethyl radical is even expected to be perpendicular to the plane in the HY case, necessitated by its closer distance of approach (1.09 Å in HY vs 2.6 Å in NaY).

Not established here is the possible role played by tunneling rotation, which is believed to be important for the ethyl radical at temperatures below about 50 K.[25] The reduced symmetry of the $-CH_2Mu$ group would likely decrease favorable wave function overlap for coherent tunneling, as would the binding of the Mu−ethyl radical to zeolite sites, but this might be offset by the much lighter Mu mass. Even so, from ref 25, the splitting of the ESR spectrum due to CH_3-group tunneling appears only for the $CH_3\dot{C}H_2$ radical formed by H-atom abstraction from C_2H_6, and not for H-atom addition to C_2H_4, which is the isotopic analogue of MuC_2H_4 formation. It can also be commented that, where tunneling rotation is believed to be important, the L parameter in the McConnell relation of eq 6 is assumed to be zero, which would be inconsistent with the data reported here.

The theoretical approaches outlined above describe only the *trends* in the measured muon Hfc's. A calculation of the *absolute* isotropic muon Hfc's for the Mu−ethyl radical in NaY has been carried out by Ghandi et al.,[49] using a B3LYP hybrid density functional and the T-atom model described earlier, at a loading of 1/sc. In lieu of a rigorous calculation of the temperature dependence of Hfc's from a Boltzmann weighting of different vibrational states at each point on the PES for torsional motion, as in the calculations of Chipman[23] and of Webster and Buttar for the muoniated ethyl radical, including anharmonicity corrections,[66] Ghandi et al. have considered only the three conformations at the energy minima along the surface (one where the C−Mu bond eclipses the p_z orbital and two where the C−H bonds do) and weighted these by a Boltzmann distribution. This naturally gives less weight to the Mu conformer at the higher temperatures, consistent with eq 6, and produces the solid line shown in Figure 12, in comparison with the experimental data points (a limited data set was shown in ref 49). The experimental values are *remarkably* well reproduced, with a maximum deviation of only 5%, seen at the lowest temperatures.

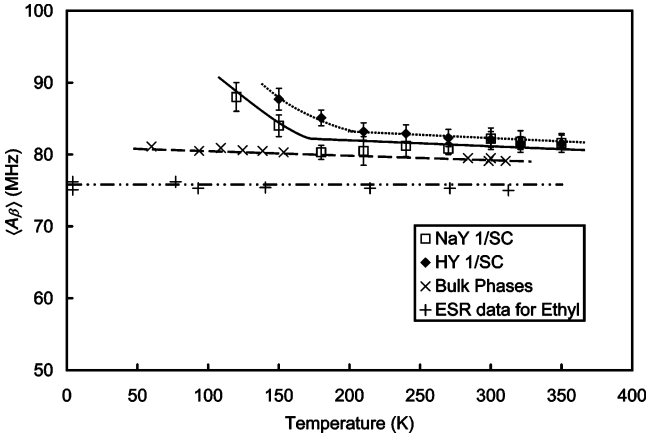

Figure 13. Plots of the *average* muon Hfc's at the β carbon, $\langle A_\beta \rangle(T)$, for the Mu−ethyl radical in HY (dotted line) and NaY (solid line) from this work, compared with similar data in the bulk (dashed line)[19,20] and with the ESR data for the unsubstituted ethyl radical (dash-dot-dot line and vertical crosses).[24−26] The lines are again drawn to indicate the trends, though the slopes for the μSR data have been assumed to all be the same at the higher temperatures.

The exemplary agreement seen between theory and experiment in Figure 12 seems almost too good, in comparison with several accurate ab initio calculations reported elsewhere on small radicals in the gas phase,[67,68] and in particular for the β protons of the ethyl radical itself.[23,27,67] These kinds of calculations provide agreement with experimental proton Hfc's at the ∼10−20% level, at best, and are strongly influenced by basis set size, different choices of configuration interactions, and density functionals. One would expect the calculation of Hfc's in the zeolite environment to be less accurate, where both cluster size and guest−host interaction potentials provide additional complications. The fact that the DFT calculations (and T-atom model) of ref 49 for the isotropic muon Hfc's in NaY works so well certainly speaks in its favor, but also suggests that its success is partly due to a cancellation of contributing errors, not uncommon in density functional theory. Nevertheless, it can also be noted that DFT calculations have been quite successful in reproducing experimental Hfc's, including those from μSR studies in different environments.[34,63]

4.3. Temperature Dependence of the Proton Hfc's, $A_\beta(T)$ and $A_\alpha(T)$. The Hfc's of the β protons plotted in Figure 9 increase with increasing temperature in a similar manner in the NaY, HY, and bulk ($\gtrsim$100 K) environments and exhibit just the opposite T dependence to $A_\mu'(T)$. This is a further consequence of C−C bond rotation, here aligning the C−H bond of the $-CH_2Mu$ group with the electron p_z orbital. At the lower temperatures, the μSR data in the bulk[19] (crosses and dashed line) deviate from the linear trend shown at higher temperatures toward the calculated value in vacuum at 0 K (37.0 MHz) from Ghandi et al.[49] This is almost the same as the calculated value for the ethyl radical at 0 K in NaY (37.5 MHz), which is the open square (with inserted cross) shown on the axis. The NaY β Hfc's at low temperatures might well accommodate the same trend as in the bulk, but the experimental line widths become too broad at temperatures below 120 K to be observed.

At the higher temperatures, both the data points and the trend lines shown in Figure 9 are seen to approach the ESR value of $A_p(\infty) = 75.3$ MHz for the CH_3 group of the unsubstituted ethyl radical. This can be seen as well in Figure 13, which plots the T dependence of the *average* values of the β proton Hfc's for the $-CH_2Mu$ group in NaY and HY, defined by

$$\langle A_\beta \rangle = 1/3(A_\mu' + 2A_\beta) \qquad (8)$$

compared again with the bulk μSR data[19] and also with the ESR data.[24−26] The guide lines for all the μSR data have been drawn with the same, slightly negative (ca. −0.008 MHz/K) slope at higher temperatures. This differs marginally from the ESR data, which, though consistent with being T independent (at 75.3 MHz), as expected, also accommodates the slightly positive slope drawn. The 5 MHz difference with the bulk μSR data is the residual isotope effect noted earlier. The μSR slopes approach the ESR value at temperatures around 1000 K, consistent with the trends in Figure 9, and well above the activation barriers for C−C bond rotation previously determined (Figure 11). This can be taken as further evidence that C−C bond rotation of Mu−ethyl is largely unimpeded by its binding to zeolite sites, also in accord with our earlier assumption of the free rotation limit being an isotopic invariant.

The temperature dependences of the α proton Hfc's for the MuC_2H_4 radical, $A_\alpha(T)$, for NaY and HY plotted in Figure 10, are also compared with the bulk μSR and ESR data for the ethyl radical. The negative signs are noteworthy, as previously commented on (eq 5). These data show more marked differences compared to the bulk than was the case for the β protons, particularly for HY, with Hfc's some 20% higher at the lower temperatures and with a similar trend to that reported in silica powder,[40] where binding to OH groups is also expected. Since little or no isotope effect is expected for the α-protons, consistent with the essentially overlapping ESR and bulk μSR data, the relatively large shifts in Hfc's seen for Mu−ethyl in HY suggest an appreciable distortion of the radical center from planar geometry at the α carbon.

From the silica powder data of ref 40, it is suggested that the binding of MuC_2H_4 to −OH sites could cause an enhanced 2s component in the sp^2-hybridized electron orbital, increasing $A_\alpha(T)$ at lower temperatures. A similar effect may be occurring in the HY environment. A geometrical distortion, with an appreciable ($\phi \neq 0$) bend angle, would also correspond to more positive values for A_α,[23] as observed. Support for such distortion is found in the calculations of ref 49, where the bond angle at the C_α position, particularly for the O4H site, is almost tetrahedral.

The calculations of ref 49 also provide some guidance for the interpretation of the α proton Hfc's for the ethyl radical in NaY. At 0 K A_α is calculated to be −33 MHz, which is the basis of the arrow shown at the end of the guide line in Figure 10, drawing then a clear distinction from the values in the bulk, which would otherwise not be apparent from the data points themselves. This rather marked difference, in contrast to the close similarity commented on earlier for the β proton Hfc's (Figure 9), is a further indication of distortion of the radical at the α carbon, arising in this case from its coupling to the S_{II} cation. The degree of distortion appears to be less in NaY than in HY though, where the calculated bond angle (116°) is much closer to planarity.[49]

4.4. Hyperfine Anisotropy and ALC-μSR Line Widths. The hyperfine contribution to the spin Hamiltonian for electron ($\mathbf{S}_e$) and muon ($\mathbf{I}_\mu$) is of the form $\mathbf{S}_e \cdot \mathbf{A}_\mu \cdot \mathbf{I}_\mu$, where $\mathbf{A}_\mu$ is a generalized (anisotropic) hyperfine coupling tensor, with a similar contribution for nuclear, here proton, spins, $\mathbf{A}_p$. In addition to a relative orientation between $\mathbf{A}_\mu$ and $\mathbf{A}_p$, there is as well an orientation of the spins with an external field, giving rise to an angle dependence for the effective isotropic Hfc's, $\tilde{A}_\mu = A_\mu(\theta,\phi)$ (and $\tilde{A}_p$), such that both the positions and the widths of ALC resonances will be angle dependent in a single crystal,[54,59] as outlined earlier. In the zeolite environment, the superposition of single-crystal spectra, each with a different

angle to the field, gives rise to powder patterns for the ALC resonances. Simulations of the powder line shapes for both the Δ_1 and Δ_0 resonances for a *static* MuC_6H_6 radical show them to be symmetric, a consequence of the "planar'' nature of the radical where one hyperfine component is much less than the other two.[31,37] Though non-Lorentzian, these static line shapes are still amenable to fitting by phenomonological Gaussian or Lorentzian line shapes, as employed in our earlier study of MuC_6H_6 in NaY.[35,36] The same assumption is made here for MuC_2H_4 in faujasites, as commented on earlier, and as shown by the fits to the ALC spectra given earlier (Figures 3, 4, and 5).

In many cases of practical interest, rapid rotation about a particular (Z) axis leads to a partial averaging of the hyperfine tensor, so the dipolar components (D_{ii}) then have the *axial* form $D_{XX} = D_{YY} = D_\perp$ and $D_{ZZ} = D_\parallel$, such that $D_\perp = -1/2D_\parallel$. For the MuC_6H_6 radical in the bulk, fast uniaxial rotation about the axis normal to the radical plane gives the axial components $D_\parallel = -2D_\perp = -6.8$ MHz.[31,59]

For the ethyl radical, the hyperfine tensors for both the α and β protons are axial, even at 4 K.[23,24,27,31,60] An axial hyperfine tensor for the ethyl radical is also facilitated by facile C−C bond rotation, in accord with its temperature-independent isotropic Hfc's.[25,26] From Chipman's calculations for the unperturbed radical,[23] for the α protons of the methylene group, $D_{ZZ}^{\alpha} = D_\parallel^{\alpha} = -6.7$ G, and for the β protons of the methyl group, $D_\parallel^{\beta} = 2.5$ G, both in quite good agreement with experiment.[23−25] In their calculations for the β protons of the ethyl radical, Ghandi et al.[49] also assume an axial tensor, and find 2.7 G at 0 K (in vacuum) for $D_\parallel^{\beta}$ almost the same value as Chipman's. For the *muon* of the $-CH_2Mu$ group, however, it is important to note that the hyperfine anisotropy will scale with γ_μ/γ_p, in like manner to its isotropic Hfc's, leading to the expectation that $D_\parallel^{\beta,\mu} = 8.6$ G or 24 MHz in the bulk, almost 4 times larger (and of opposite sign) than the −6.8 MHz value given above for MuC_6H_6.

One would nominally expect the hyperfine anisotropy of a radical in the zeolite to be similar to that in the bulk, since the hyperfine tensor is defined by the body-fixed geometry of the radical, an assumption that was made in ref 35 for MuC_6H_6 in NaY (though later analysis of higher temperature data relaxed this constraint[36]). From the calculations of ref 49 though, a considerable difference in hyperfine anisotropy is found between the vacuum (bulk) and the NaY environment for Mu−ethyl, giving $D_\parallel^{\beta,\mu}$ (NaY) =13.0 G (or 36.5 MHz), with a huge effect at the O4H site in HY, $D_\parallel^{\beta,\mu}$ (HY) = 24.0 G (or 68 MHz). Since the *widths* of the Δ_1 ALC-μSR lines depend on the degree of hyperfine anisotropy, considerably broader lines for the MuC_2H_4 radical in NaY than those reported earlier for MuC_6H_6 in ref 35 can be expected, with even larger widths for MuC_2H_4 in HY.

4.4.1. The Δ_1 Resonances: Mu−Ethyl Molecular Motion. Since, as outline above, the ethyl radical itself exhibits an axial hyperfine tensor and since this is also the assumption made in the calculations of ref 49 for its Mu-substituted analogue, it is important to examine the ALC-μSR shapes expected on the basis of this assumption. In a single-crystal environment, the form of the time-integrated ALC muon polarization for an axial hyperfine tensor for the Δ_1 resonance has the form[59]

$$\overline{P_z}(B,\theta) = 1 - \frac{0.5{q_1}^2{P_z}^0}{\lambda^2 + {q_1}^2 + (\nu_\mu - {\nu_\mu}^0)^2} \qquad (9)$$

where P_z^0 is the initial muon polarization, usually assumed to be unity, λ (in μs^{-1}) is due to muon decay, as well as any additional chemical relaxation processes that take the muon out of resonance (i.e., $\nu_\mu \neq \nu_\mu^0$), and $q_1 = 3/2D_\perp \cos\theta \sin\theta$ is the angle dependence arising from the form of the operators $\mathbf{S}_z^e \mathbf{I}_+^\mu$ that induce a muon spin flip. It is worth noting that when $\langle q_1 \rangle$ averages to zero as a result of fast isotropic reorientation, as in the gas phase,[20,33,55] (or if $D_\perp$ itself were zero), that the Δ_1 resonance completely disappears,

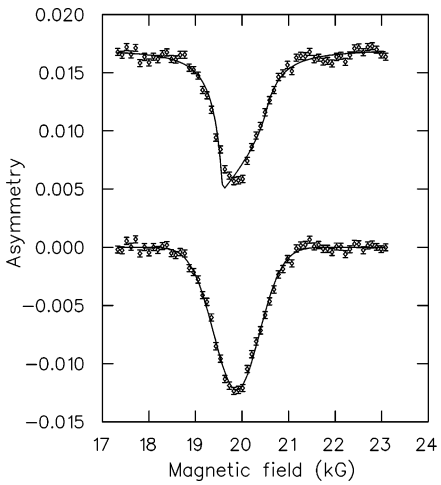

Figure 14. The results of a powder fit for an axial hyperfine tensor to the data for the Mu−ethyl radical in NaY at 6 K (top), with λ fixed at the inverse of the muon lifetime (0.45 μs^{-1}), compared with the Gaussian fit shown earlier in Figure 3 (bottom). Note the characteristic "cusplike'' shape to the axial powder fit. The fitted width is $D_{ZZ} = D_\parallel$ = 15.9 MHz (>0 for a prolate shape) or Γ (fwhm)= 1170 G, which is the same width as for the Gaussian fit ($\Gamma = 2.35\sigma$). The axial powder fit does not account for the symmetric nature of the minimum nearly as well as the Gaussian fit does and also gives a poor overall χ^2.

In the zeolite polycrystalline environment, the superposition of different angles contributing to eq 9 leads to a *nonsymmetric* powder pattern for the Δ_1 line, with a distinct "cusplike'' shape.[35,37,54,59] In the case of MuC_6H_6, the clearest evidence for such asymmetric shapes has been seen in the silicious environment of ZSM-5,[37] with a pattern characteristic of an *oblate* rotor ($D_\parallel < 0$). Were the Mu−ethyl radical to also exhibit an axial hyperfine tensor for the $-CH_2Mu$ group, similar cusplike line shapes for the Δ_1 resonances would be expected but with broader line widths due to the increased hyperfine anisotropy discussed above for MuC_2H_4. The pattern should also have the opposite orientation since rotation about the C−C bond axis gives a *prolate* shape ($D_\parallel > 0$).

Figure 14 gives the result of such a powder-pattern fit (λ fixed at the inverse of the muon lifetime, 0.45 μs^{-1}) for the Δ_1 resonance of Mu−ethyl in NaY at 6K (top), compared with the Gaussian fit from Figure 3 (bottom). The cusplike shape is clearly seen in the powder-pattern fit but not in the data, and the fit is particularly poor in the region of the minimum. The fitted value for $D_\parallel$ is 15.9 MHz (for a prolate shape, as anticipated), about half the 36 MHz expected from the muon anisotropy in the calculations of ref 49. (Fixing $D_\parallel$ at 36 MHz gives a much worse fit.) A similar attempt to fit the HY data gave almost the same fitted value for $D_\parallel$ as in NaY, in contrast to the factor of 2 difference expected from the calculations of hyperfine anisotropy for Mu−ethyl at the O4H site in HY. The Gaussian fit shown in the bottom of Figure 14 gives a much better account of the data (and similarly so in HY). Though an enhanced relaxation rate, λ from eq 9, would broaden the axial line shape, rendering it more symmetric, there is no obvious mechanism for such enhancement, particularly at 6 K. We

conclude that the hyperfine tensor for the MuC_2H_4 radical in NaY (HY and USY) is most likely *not* axial, consistent with the phenonomological Gaussian fits of Figures 3−5. Nevertheless, it is noted that the width of the axial-tensor fit of Figure 14, giving a fwhm of $\Gamma = D_{ZZ}/\gamma_\mu = 1170$ G, is the same as that found from the Gaussian fit (Table 1), $\Gamma = 1175$ G (fwhm $= 2.35\sigma$). Similar symmetric line shapes, with somewhat narrower but comparable widths, were seen at lower temperatures for the MuC_6H_6 radical interacting with cation sites in NaY,[35] qualitatively consistent with the differences in hyperfine anisotropies noted above.

In marked contrast to the MuC_6H_6 data in NaY though, the widths of the Δ_1 resonances for MuC_2H_4 increase markedly with increasing temperature, in both NaY and HY, from ∼1000 G at the lower temperatures to ∼2000 G near 200 K (Tables 1 and 2), and then become too broad to fit, merging with the baseline as room temperature (RT) is approached. In USY the line shapes are also symmetric but the widths are more constant with temperature, though again increased broadening is seen at the highest temperatures (Table 3). As mentioned earlier, this is likely a legacy of the higher sample preparation temperatures employed in these samples, but it could also be partly due to the reduced number of OH sites in USY (Si/Al ∼ 15) giving enhanced broadening due to a nonuniform distribution of Al atoms.[69]

That the Δ_1 ALC-μSR lines for Mu−ethyl broaden significantly with *increasing* temperature in particularly NaY and HY suggests a mechanism of isotropic reorientation,[57,58] demonstrated previously for the MuC_6H_6 radical translating around the spherical grains of silica powder[56,57,70] and in the case of rotating C_{60} molecules (in contrast to C_{70}),[71] but not previously established in zeolites.

Though the tensor is nonaxial, the components of the axial tensor can still reasonably be used to set the time scale for molecular motion. Thus reorientation in times comparable to the inverse of the hyperfine anisotropy, $\tau_{ALC} \sim 1/(2\pi D_\perp)$, ≈ 10 ns for Mu−ethyl, from the calculations of ref 49 (and ≈50 ns for MuC_6H_6[31,35,37]), partially averages out the hyperfine anisotropy. As the fraction of the muon ensemble aligned with the field direction decreases at higher temperatures, the resonance begins to disappear through enhanced broadening. With faster and faster jump times, the Δ_1 line gets so broad as to disappear into the baseline.[57,58] In the limit of fast isotropic motion, on a time scale $\tau_c \ll \tau_{ALC}$, the Δ_1 resonance averages completely to zero, leaving only the Δ_0 resonance as an observable,[37,57,59] an important signature for molecular motion. This is exactly the behavior observed in the present data, where both Δ_0 resonances become prominent at those temperatures where the Δ_1 lines are disappearing (see, e.g., Figure 4) and suggests in turn that the Mu−ethyl radical begins to desorb from its binding sites at temperatures even below RT.

We can estimate the activation energy for this desorption from a simple Arrhenius model, $\tau_c = \tau_0 e^{E_D/RT}$, where τ_c is the correlation time for reorientation of the radical, and τ_0 corresponds to a typical time for molecular rotation, ≈0.1 ps. Since the Δ_1 signals are highly broadened by 200 K in both NaY (Figure 3) and HY (Figure 4), we assume that $\tau_c \sim \tau_{ALC} \approx 10$ ns at this temperature, giving an activation energy for desorption of $E_D \sim 20$ (±5) kJ/mol, in both NaY and HY. At RT, τ_c would then be ∼0.3 ns, $\ll\tau_{ALC}$, in accord with the loss of the Δ_1 resonance near this temperature.

This model implies isotropic reorientation of a desorbed ethyl radical within a supercage, but the value of $E_D \sim 20$ kJ/mol found for the activation energy seems far too low for such a process, in comparison with the BE calculations of Ghandi et al., of ∼137 kJ/mol at S_{II} cations in NaY, and even more so compared to ∼327 kJ/mol at O4H sites in HY. This in turn suggests that the ethyl radical does not completely desorb from its binding sites but rather underoes fast reorientational "hops'' from site to site within the tetrahedral environment of the supercage. Such a hopping motion between equivalent sites could also correspond to isotropic reorientation and would not be distinguished by this simple model. If the hop rate is fast enough, faster than the lattice relaxation, it may well be that the activation energy for desorption is much less than the BE.

The presence of localized electron density centered on the α carbon gives rise to an electric dipole moment $\mu_E = 0.25$ D for the ethyl radical (not reported in ref 49) and correspondingly a dipolar interaction energy with the NaY cluster (at $r = 2.6$ Å) of ∼22 kJ/mol. A similar value was reported earlier by Macrae and Wester for the MuC_6H_6 radical in NaY ($\mu_E = 0.49$ D but at $r = 3.1$ Å).[63] This dipolar energy for Mu−ethyl is the same as the activation energy found from the model above for desorption in NaY, supporting a fast hopping mode as being largely responsible for the broadended Δ_1 line widths seen. A similar dipolar interaction energy of MuC_2H_4 with the −OH groups and nearby charge on the HY framework could be expected, consistent with the range of desorption energies found experimentally.

The behavior seen though for MuC_2H_4 in both NaY and HY, where the Δ_1 lines for MuC_2H_4 broaden to such an extent as to merge into the baseline near 300 K, stands in sharp contrast to that seen for the MuC_6H_6 radical in NaY,[35,36] where the Δ_1 lines are stable up to 470 K, reflecting the relatively strong binding of the radical to S_{II} cation sites in particular. This, along with the aforementioned dipolar interaction energy of ∼22 kJ/mol serves to "lock'' the cyclohexadienyl radical in place, providing an explanation of the largely *static* ALC line widths seen for MuC_6H_6 in NaY. However, such a view poses a conundrum in comparison with the present study. Why, with a similar dipolar interaction energy but an expected much stronger BE of ∼137 kJ/mol,[49] is there not at least a similar degree of immobility for MuC_2H_4 in NaY as for MuC_6H_6 over a comparable temperature range and even more so for HY? It may be that the calculated BEs for MuC_2H_4 in ref 49 are too large, as alluded to earlier, or perhaps, C−C bond rotation coupled with the distortion of the radical at C_α faciliates desorption for the ethyl radical in contrast to the in-plane rotation of the cyclohexadienyl radical.

Since molecular motion and/or exchange between sites is a prerequisite for any chemical reaction within the micropores of zeolites, the highly broadened line widths seen experimentally for the Δ_1 resonances of MuC_2H_4 in both NaY and HY indicate that the ethyl radical might well be a contributing intermediate in catalyzed hydrocarbon cracking processes, in contrast to the largely static Mu−cyclohexadieynl radical. That the MuC_6H_6 radical is rendered largely immobile by its strong binding to Na cations in NaY is not overly surprising, since it is known from other studies that molecular dynamics of benzene itself is hindered in NaY compared to HY (or USY).[72] However, it is then again puzzling why the Mu−ethyl radical exhibits such similar behavior in NaY and HY, which only reinforces the conundrum posed above.

4.4.2. The TF-μSR Relaxation Rates. The enhanced molecular motion indicated by the broadening of the Δ_1 lines for the Mu−ethyl radical discussed above is paralleled by the increased FT-μSR line widths seen in NaY with increasing temperature in Figure 2. These are most intense and sharp near ∼180 K, where the Δ_1 ALC lines begin to broaden appreciably.

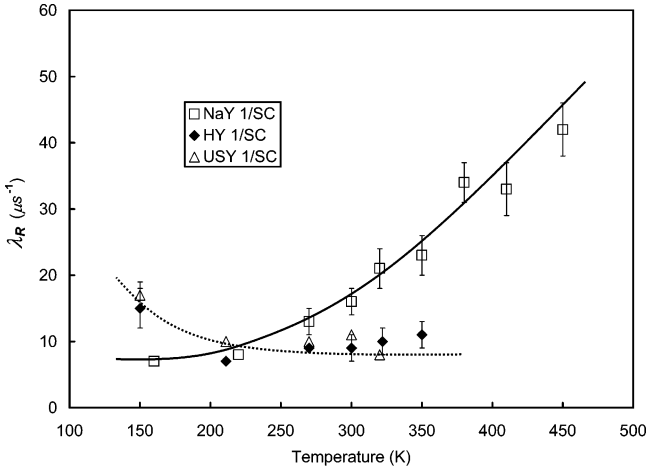

Figure 15. A plot of the TF relaxation rates, λ_R, for the MuC_2H_4 radical vs temperature in NaY (solid line) and HY/USY (dotted line), from fits to the time dependence of the muon asymmetry in four separate histograms (averaged), from eq 1. The error bars shown also include an estimate of systematic error. The curves shown are again guides to the eye. Significantly, at higher temperatures, the relaxation rates in HY/USY are *T* independent, but for NaY these continue to increase, suggesting further interactions of the Mu−ethyl radical with Na cations.

The broadening and asymmetric line shapes seen at lower temperatures are due to hyperfine anisotropy in a polycrystalline environment,[31,53] but the increased broadening and similar line shapes seen at the higher temperatures were unexpected and indicate some further interaction of weakly bound or desorbed MuC_2H_4 with the zeolite structure or framework nuclear moments. (A similar mechanism likely contributes to the fast relaxation rates seen in TF studies of Mu in zeolites.[28]) If due to the Al nuclear moments, which have a complex distribution in Y-zeolites,[69] the larger Si/Al ratio in USY should give rise to reduced relaxation rates compared to HY, but this is not the case, as can be seen in Figure 15, which plots the time-differential relaxation rates for Mu−ethyl, λ_R (a weighted average of four separate histograms, from fits to eq 1) vs temperature. The results in HY/USY are the same, with relaxation rates that decrease slightly with increasing temperature, in contrast to the results in NaY, where λ_R continues to increase with temperature, and quite dramatically so above about 250 K. Since the Si/Al ratio is the same in the NaY and HY samples (Si/Al = 2.5) and very different in the USY sample (Si/Al = 15), both the similarity in λ_R values for HY and USY, and their marked difference compared to NaY, rules out Al nuclear moments as making any significant contribution to these higher-temperature TF relaxation data.

This suggests in turn that the enhanced TF relaxation rates seen for the Mu−ethyl radical in NaY is due to a dipolar interaction with the extraframework Na nuclear moments and/or to electron transfer from $MuCH_2\dot{C}H_2$ to the Na cations, causing a spin-dephasing in the radical, a process which could also contribute to the enhanced broadening of the ALC lines seen in Figure 3.[57] From the calculations of ref 49, a Na Hfc of 156 Mz (at 0 K) is expected, which would correspond to an appreciable transfer of electron spin density to the Na of about 15%. It is also commented that the Δ_1 ALC lines persist to higher temperatures in HY/USY (Figures 3 and 4), where no corresponding spin transfer is possible.

4.4.3. The Δ_0 Resonances and Proton Hfc's. Though the main contribution to a Δ_0 resonance arises from the *isotropic* hyperfine interaction, via "flip-flop'' coupling terms involving the operators $\mathbf{S}^e_- \mathbf{I}^\mu_+$ and $\mathbf{S}^e_+ \mathbf{I}^p_-$, these same terms also arise from the *anisotropic* (dipolar) part of the interaction, with a contribution proportional to $q_0 = D_\perp(1 - 3\cos^2\theta)$.[31,59] Were the hyperfine tensor axial, integration of the muon polarization over time for a single crystal leads to an expression for the Δ_0 resonance similar to that of eq 9 for the Δ_1 case,[57,59] but with the angle dependence above. In the zeolite polycrystalline environment, the powder pattern would again give asymmetric cusplike ALC-μSR line shapes.[35,37,59] Like the Δ_1 resonances though, the present data for both the α and β Δ_0 resonances of Mu−ethyl are largely symmetric (Figures 5 and 4), also in accord with a nonaxial hyperfine tensor.

As with the Δ_1 case, we can expect the ALC line widths for the Δ_0 resonances (Tables 1−3) to reflect the hyperfine anisotropy. However, there is an additional contribution (to q_0) arising from the isotropic hyperfine coupling,[53,55,57] which is proportional to $A_\mu A_p/B_r\gamma_e$ (ignoring electron relaxation), where B_r is the resonant condition of eq 5. This effect contributes to the Δ_0 lines being less sensitive to molecular dynamics than Δ_1, which are observed only in anisotropic environments. Since the β proton resonance falls at a lower field (as in Figure 5), this isotropic contribution would broaden the β resonance by ∼25% compared to the α proton one, as seen in the gas phase.[20,55]

However, in the zeolite environment, since the α proton hyperfine anisotropy is some 3-fold larger than that for the β protons,[23,27] we would expect much broader lines for the α proton Δ_0 resonances. (Werst et al.[11] have also commented that hyperfine anisotropy particularly broadens the α proton ESR lines of the ethyl radical in NaZSM-5.) That there is little difference (outside scatter) in the measured widths of the α and β lines for Mu−ethyl in faujasites, over most of the temperature range, suggests some enhanced dynamics contribution to the widths for the β proton resonances, in accord with the enhanced broadening for the Δ_1 resonances discussed above. Even so, at the highest temperatures in NaY, the α proton resonances are consistently much broader (Table 1 and Figure 5), which likely is at least partly due to the degree of electron spin transfer noted above between the MuC_2H_4 radical and the sodium cation.

5. Summary Remarks

The present paper reports on μSR measurements of the Hfc's and the widths of avoided level crossing resonances for the MuC_2H_4 radical in the faujasites NaY, HY, and USY, the first study of its kind and, to our knowledge, the first such study of the ethyl radical in zeolites by *any* technique. The motivation was 2-fold. First, to compare with earlier similar investigations of the MuC_6H_6 radical in NaY, where unprecedented shifts in both muon and proton Hfc's compared to bulk values and to silicious environments had been determined, and where the ALC line widths indicated largely *static* radicals over a wide range of temperatures.[35,36] It remained to be seen whether the same effects would be seen for a prototypical Mu−alkyl radical. Second, to compare with theory and particularly with the recent calculations of ref 49 for the binding energies and hyperfine couplings of the Mu−ethyl radical in both NaY and HY. Several important points emerge within this context, in comparison as well with previous studies of MuC_2H_4 in the bulk phase.

In sharp contrast to the observations of multiple ALC-μSR resonances for the Mu−cyclohexadieynl radical in NaY, due to its binding to both S_{II} cation and window sites, only *three* ALC-μSR resonances are seen for Mu−ethyl in NaY (and in HY and USY), one muon (Δ_1) resonance and two Δ_0 resonances, for β and α proton hyperfine couplings. There is no evidence for other than a single site being populated in each framework and, in particular, no evidence for Mu−ethyl residing at window sites, in contrast to MuC_6H_6 in NaY.

In all three frameworks, the *muon* Hfc's for MuC_2H_4 at the lowest temperatures, in the region of the "McConnell plateau'', are about 10% above those found in the bulk (Figures 7 and 8). Though this shift is only half that reported earlier for MuC_6H_6 in NaY, it is still appreciable and in like manner is interpreted as evidence for binding of the ethyl radical to specific zeolite sites: to the S_{II} cation sites in NaY and to framework hydroxyls in HY (and USY). Despite the different nature of their binding sites though, there is little or no framework dependence seen in the muon Hfc's, and as well only modest evidence for some loading dependence in HY (Figure 8).

The T dependence of the reduced muon Hfc's, $A_\mu'(T)$, follows much the same trend as in the bulk (or on silica powder), decreasing with increasing temperature, as expected from the rotation of the C−Mu bond away from its favorable "eclipsed'' overlap with the p_z orbital at 0 K. An Arrhenius fit (Figure 11) gives activation barriers for this torsional motion of ∼1200 J/mol, independent of zeolite environment and essentially the same value as found in the bulk. It is somewhat surprising that C−C bond rotation is so little affected by binding of the Mu−ethyl radical to zeolite sites; indeed, at the higher temperatures, it appears to be as facile as in the gas phase, indicative of radical desorption.

The Hfc's for the β protons also exhibit a similar T dependences to that seen in the bulk phase, with the expected opposite trend to the muon, as the protons of the $-CH_2$ Mu group move into a more eclipsed conformation with increasing temperature. The shifts in β proton Hfc's are less dramatic than those seen for the muon at lower temperatures though (Figure 9). In contrast, the α proton Hfc's show both larger shifts at lower temperatures and an opposite T dependence compared with bulk values, increasing quite dramatically with decreasing temperature in both NaY and HY (Figure 10). Distortion of the ethyl radical geometry at the α carbon is indicated, consistent with the calculations of ref 49.

The broad and symmetric line shapes seen for the Δ_1 muon resonances of MuC_2H_4 in both NaY (Figure 3) and HY (Figure 4) are indicative of a *nonaxial* hyperfine tensor and in this regard are similar to those reported earlier for MuC_6H_6 in NaY. Attempts to fit these data at 6 K assuming an axial tensor, known to be the case for the bulk ethyl radical, were not successful (Figure 14). As in our earlier study of Mu−cyclohexadienyl in NaY, the Δ_1 line shapes for Mu−ethyl have been fit to Gaussians over the range of temperatures studied. At 6 K the line widths are about half as large as would be expected in NaY from the calculations of hyperfine anisotopy in ref 49 (and much narrower than these calculations predict in HY) though the phenomonological nature of the fits does have to be kept in mind.

The USY data are similar to those of HY, as expected for similar environments, but in contrast exhibit broader lines at lower temperatures. This is believed to be mainly due to the generally higher sample temperatures employed to drive off water of hydration, which may have introduced paramagetic defects, but could also be partly due to differing Al content in the high Si/Al (=15) enviroment.

Though the symmetric Δ_1 line shapes are similar for both MuC_2H_4 and MuC_6H_6 in NaY, the line *widths* for MuC_2H_4 increase noticeably with increasing temperature, merging with the baseline at temperatures near ∼200 K (Figures 3 and 4). This behavior contrasts sharply with that seen for the static shapes of the Mu−cyclohexadienyl radical and indicates an isotropic reorientational motion for the Mu−ethyl radical. The radical appears either to largely desorb from its binding sites or to undergo a fast hopping motion between equivalent sites in a supercage.

An Arrhenius estimate of the activation barrier for this desorption, $E_D \sim 20(\pm 5)$ kJ/mol, for both NaY and HY, is in good accord with an expected dipolar interaction energy of ∼ 22 kJ/mol between the ethyl radical and the Na cluster but is much less than the calculated BE of ∼137 kJ/mol (and even more so for sites in HY) from ref 49. A similar dipolar energy for the MuC_6H_6 radical, along with a BE of ∼40 kJ/mol, appears to "lock'' the Mu−cyclohexadieynl radical in place at cation sites in NaY, thus explaining the static line shapes seen. In the case of Mu−ethyl, with a similar dipolar energy and much larger BEs, a degree of immobility at least the same as that for MuC_6H_6 would be expected, contrary to observation (Figures 3 and 4), posing a conundrum. It may be that the much lower Arrhenius activation energy estimated here is indicative of some kind of concerted motion involving C−C bond rotation and a site-hopping reorientation of the radical as a whole, on a time scale faster than lattice relaxation times.

Though the binding energies and anisotropic Hfc's for Mu−ethyl in NaY (and HY) zeolites, from the T-atom-model and DFT calculations of Ghandi et al.[49] have been called into question by the present results, their calculations for the *isotropic* muon Hfc's of the MuC_2H_4 radical with temperature in NaY, $A_\mu'(T)$, are in excellent agreement with the experimental results, at the 5% level (Figure 12).

Increased TF time-differential relaxation rates seen at higher temperatures in NaY, shown in Figure 15, suggest additional contributions to the widths arising either from magnetic dipolar interactions with the extraframework Na nuclear moments or from a spin relaxation of the radical itself due to an appreciable (∼15%) transfer of electron spin density to the Na cation, expected from the calculations of ref 49. It is noteworthy that there is no corresponding increase in TF relaxation rates in either HY or USY.

The behavior of the Δ_1 resonances for MuC_2H_4 in NaY and HY to noticeably broaden with increasing temperature is paralleled by the appearance of much narrower β proton and α proton Δ_0 resonances near the same temperatures where the Δ_1 lines disappear (Figure 5). Since Δ_0 resonances also exist under isotropic conditions, this behavior supports the isotropic reorientation model for the MuC_2H_4 radical mentioned above. The widths of the Δ_0 lines are fairly constant at those temperatures where they are clearly seen (≳180 K, Figure 5), except at the higher temperatures for the α proton resonance in NaY, which tend to increase noticeably (Table 1). This is likely also due to interactions with Na cations, since there is again no such enhanced relaxation seen in HY or in the more siliceous USY environment (nor in the silica powder data of ref 40).

The enhanced molecular motion seen for the Mu−ethyl radical in both NaY and HY, as evidenced by the pronounced broadening of the Δ_1 resonances seen as RT is approached, suggests that the ethyl radical could well be a relevant intermediate in zeolite-catalyzed hydrocarbon cracking processes. This is in contrast to the cyclohexadienyl radical, where its muon analogue, MuC_6H_6, exhibits largely static line widths and hence little or no molecular motion over a comparable temperature range.

Acknowledgment. We acknowledge both the interest of Dr. Syd Kreitzman in this work and his management of the Center for Molecular and Materials Sciences at TRIUMF. Thanks also to two summer students, Mr. Cori Wong and Mr. Jahangir Valiani, for their help with the data taking. Helpful comments

from Dr. Rod Macrae and Dr. Paul W. Percival were appreciated, and a special vote of thanks to Dr. Emil Roduner for his comments and for his reading of an earlier version of the manuscript. D.G.F. would also like to thank the Alexander von Humboldt Stiftung for their awarding of a "wiedereinladung'', for stays at the Physical and Theoretical Chemistry Institutes of the FU Berlin and the University of Stuttgart. We also gratefully acknowledge the financial support from the Natural Sciences and Engineering Council (NSERC) of Canada.

References and Notes

(1) Haw, J. F. *Phys. Chem. Chem. Phys.* **2002**, *4*, 5431.
(2) Breck, D. W. *Zeolite Molecular Sieves*; Robert Krieger Publishing: New York, 1973.
(3) Barthomeuf, D. *Catal. Rev.* **1996**, *38*, 521.
(4) Venuto, P. B. In Progress in Zeolites and Microporous Materials. *Stud. Surf. Sci. Catal.* **1997**, *105*, 811.
(5) Jacobs, A.; Martens, J. A. In *Introduction to Zeolite Science and Practice*; van Bekkum, H., et al., Eds.; Elsevier: Amsterdam, 1991; p 531.
(6) Sastre, G.; Richard, C.; Catlow, A.; Chica, A.; Corma, A. *J. Phys. Chem. B* **2000**, *104*, 416.
(7) Correa, R. J.; Mota, C. J. A. *Phys. Chem. Chem. Phys.* **2002**, *4*, 375.
(8) Zheng, X.; Blowers, P. *J. Phys. Chem. A* **2006**, *110*, 2455.
(9) Lange, J.-P.; Gutsze, A.; Karge, H. G. *J. Catal.* **1988**, *114*, 136.
(10) Piocos, E. A.; Han, P.; Werst, D. W. *J. Phys. Chem.* **1996**, *100*, 7191.
(11) Werst, D. W.; Han, P.; Chousse, S. C.; Vinokur, E. I.; Xu, L.; Trifunic, A. D.; Erikson, L. A. *J. Phys. Chem. B* **1999**, *103*, 9219.
(12) Kaprinidis, N. A.; Landis, M. S.; Turro, N. J. *Tetrahedron Lett.* **1997**, *38*, 2609.
(13) Barbon, A.; Bellinazzi, M.; Casgrande, M.; Storaro, L.; Lenarda, M.; Brustolon, M. *Phys. Chem. Chem. Phys.* **2006**, *8*, 5069.
(14) Hill, J.-R.; Freeman, C. M.; Delley, B. *J. Phys. Chem. A* **1999**, *103*, 3772.
(15) Truong, T. N. *J. Phys. Chem. B* **1997**, *101*, 2750.
(16) Yoda, E.; Kondo, J. N.; Domon, K. *J. Phys. Chem. B* **2005**, *109*, 1464.
(17) Carley, A. F; Edwards, H. A.; Mile, B; Wyn Roberts, M; Rowlands, C. G; Hancock, F. E.; Jackson, D. S. *J. Chem. Soc., Faraday Trans.* **1994**, *90*, 3341.
(18) Fleming, D. G.; Pan, J. J.; Senba, M.; Arseneau, D. J.; Kiefl, R. F.; Shelley, M. Y.; Cox, S. F. J.; Percival, P. W.; Brodovitch, J.-C. *J. Chem. Phys.* **1996**, *105*, 7517.
(19) Yu, D. Ph.D. Thesis, Department of Chemistry, Simon Fraser University, Canada, 1990.
(20) Percival, P. W.; Brodovitch, J.-C.; Leung, S.-K.; Yu, D.; Kiefl, R. F.; Garner, D. M.; Arseneau, D. J.; Fleming, D. G.; Gonzalez, A.; Kempton, J. R.; Senba, M.; Venkateswaran, K.; Cox, S. F. J. *Chem. Phys. Lett.* **1989**, *163*, 241.
(21) Percival, P. W.; Brodovitch, J. C.; Arseneau, D. J.; Senba, M.; Fleming, D. G. *Physica B* **2003**, *326*, 72.
(22) Ramos, M. J.; McKenna, D.; Webster, B. C.; Roduner, E. *J. Chem. Soc., Faraday Trans.* **1984**, *80*, 255, 267.
(23) Chipman, D. M. *J. Chem. Phys.* **1991**, *94*, 6632.
(24) McDowell, C. A.; Raghunthan, P.; Shimokoshi, K. *J. Chem. Phys.* **1973**, *58*, 114.
(25) Toriyama, K.; Iwasaki, M.; Nunome, K.; Muto, H. *J. Chem. Phys.* **1981**, *75*, 1633.
(26) Griller, D.; Mariott, P. R.; Preston, K. F. *J. Chem. Phys.* **1979**, *71*, 3703.
(27) Carmichael, I. *J. Phys. Chem.* **1991**, *95*, 6198.
(28) Arseneau, D. J.; Fleming, D. G.; Fyfe, C. A.; Senba, M. *Physica B* **2003**, *326*, 64.
(29) Nakano, K.; Goto, K.; Pratt, F. L.; Watanabe, I.; Nozue, Y. *Physica B* **2006**, *374*−*375*, 359.
(30) Roduner, E. *Appl. Magn. Res.* **1997**, *13*, 1.
(31) Roduner, E. *Chem. Soc. Rev.* **1993**, *22*, 337.
(32) Roduner, E.; Strub, W.; Burkhard, P.; Hochmann, J.; Percival, P. W.; Fischer, H.; Ramos, M.; Webster, B. C. *Chem. Phys.* **1982**, *67*, 275.
(33) Fleming, D. G.; Arseneau, D. J.; Pan, J. J.; Shelley, M. Y.; Senba, M.; Percival, P. W. *Appl. Magn. Res.* **1997**, *13*, 181.
(34) Percival, P. W.; Addison-Jones, B.; Brodovitch, J-C.; Ghandi, K.; Schth, J. *Can. J. Chem.* **1999**, *77*, 326.
(35) Fleming, D. G.; Shelley, M. Y.; Arseneau, D. J.; Senba, M.; Pan, J. J.; Roduner, E. *J. Phys. Chem. B* **2002**, *106*, 6395.
(36) B. Beck, Ph.D. Thesis, Department of Physical Chemistry, Universitt Stuttgart, Germany, 2003. Beck, B.; Roduner, E.; Fleming, D. G.; et al. paper in progress.
(37) Roduner, E.; Stolmar, M.; Dilger, H.; Reid, I. D. *J. Phys. Chem.* **1998**, *102*, 7591.
(38) Roduner, E.; Dilger, H. *J. Am. Chem. Soc.* **2001**, *123*, 7717.
(39) Rhodes, C. J.; Dintinger, T. C.; Scott, C. A. *Magn. Res. Chem.* **2000**, *38*, 62.
(40) Schwager, M.; Roduner, E.; Reid, I. D.; Percival, P. W.; Brodovitch, J.-C.; Wlodek, S.; Marzke, R. F. *Hyperfine Interact.* **1994**, *87*, 859.
(41) Zhao, G.; Gross, B.; Dilger, H.; Roduner, E. *Phys. Chem. Chem. Phys.* **2002**, *4*, 974.
(42) Simon, J.-M.; Bellat, J.-P.; Vasenkov, S.; Krger, J. *J. Phys. Chem. B* **2005**, *109*, 13523.
(43) Henson, N. J.; Eckert, J.; Hay, P. J.; Redondo, A. *Chem. Phys.* **2000**, *261*, 111.
(44) Hbner, G.; Rauhut, G.; Stoll, H.; Roduner, E. *Phys. Chem. Chem. Phys.* **2002**, *4*, 3112.
(45) Beauvais, C.; Guerrault, X.; Coudert, F.-X.; Boutin, A.; Fuchs, A. *J. Phys. Chem. B* **2004**, *108*, 399.
(46) Jousse, F.; Auerbach, S. M.; Vercauteren, D. P. *J. Phys. Chem. B* **2000**, *104*, 2360.
(47) Evleth, E. M.; Kassub, E.; Jessri, H.; Allavena, M.; Montero, L.; Sierra, L. R. *J. Phys. Chem.* **1996**, *100*, 11368.
(48) Limtrakul, J.; Nanok, T.; Jungsuttiwong, S.; Khongpracha, P.; Truong, T. T. *Chem. Phys. Lett.* **2001**, *349*, 161.
(49) Ghandi, K.; Zahariev, F. E.; Wang, Y. A. *J. Phys. Chem. A* **2005**, *109*, 7242.
(50) Beta, I. A.; Bhlig, H.; Hunger, B. *Phys. Chem. Chem. Phys.* **2004**, *6*, 1975.
(51) Maurin, G.; Bell, R. G.; Devautor, S.; Henn, F.; Giuntini, J. C. *J. Phys. Chem. B* **2004**, *108*, 3739.
(52) Duchovic, R. J.; Wagner, A. F.; Turner, R. E.; Garner, M. D.; Fleming, D. G. *J. Chem. Phys.* **1991**, *94*, 2794.
(53) Heming, M.; Roduner, E. *Surf. Sci.* **1987**, *535*, 189−190. Heming, M. *Z. Phys. Chem.* **1987**, *151*, 35.
(54) Martyniak, A.; Dilger, H.; Scheuermann, R.; Tucker, I. M.; McKenzie, I.; Vujosevic, D.; Roduner, E. *Phys. Chem. Chem. Phys.* **2006**, *8*, 1.
(55) Dilger, H.; Roduner, E.; Stolmar, M.; Reid, I. D.; Fleming, D. G.; Arseneau, D. J.; Pan, J. J.; Senba, M.; Shelley, M. *Hyperfine Interact.* **1997**, *106*, 137.
(56) Roduner, E.; Schwager, M.; Tregenna-Piggott, P.; Dilger, H.; Shelley, M.; Reid, I. D. *Ber. Bunsen-Ges. Phys. Chem.* **1995**, *99*, 1338.
(57) Kreitzman, S. R.; Roduner, E. *Chem. Phys.* **1995**, *192*, 189. Kreitzman, S. R. *Chem. Phys.* **1991**, *154*, 353.
(58) Tregenna-Piggott, P. L. W.; Roduner, E.; Santos, S. *Chem. Phys.* **1996**, *203*, 317.
(59) Roduner, E. *Hyperfine Int.* **1990**, *65*, 857. Roduner, E.; Reid, I. D.; Ricco, M.; De Renzi, R. *Ber. Bunsen-Ges. Phys. Chem.* **1989**, *93*, 1194.
(60) Atherton, N. M. *Principles of Electron Spin Resonance*; Ellis Horwood and Prentice Hall: New York, 1993.
(61) Heming, M.; Roduner, E.; Patterson, B. D.; Odermatt, W.; Schneider, J.; Baumeler, H.; Keller, H.; Savic, I. M. *Chem. Phys. Lett.* **1986**, *128*, 100.
(62) Fitch, A. N.; Jobic, H.; Renouprez, A. *J. Phys. Chem.* **1986**, *90*, 1311.
(63) Macrae, R. M.; Webster, B. C. *Physica B* **2003**, *326*, 68. Webster, B.; Macrae, R. M. *Physica B* **2000**, *289*−*290*, 598.
(64) Fuchs, A. H.; Cheetham, A. K. *J. Phys. Chem. B* **2001**, *105*, 7375.
(65) Claxton, T. A.; Graham, A. M. *J. Chem. Soc., Faraday. Trans. 2* **1987**, *83*, 2307.
(66) Webster, B.; Buttar, D. *J. Chem. Soc., Faraday Trans.* **1996**, *92*, 2331.
(67) Perera, S. A.; Salemi, L. M.; Bartlett, R. J. *J. Chem. Phys.* **1997**, *106*, 4061.
(68) Rinkevicius, Z.; Telyatnyk, L.; Vahtra, O.; Agren, H. *J. Chem. Phys.* **2004**, *121*, 7614.
(69) Jiao, J.; Kanellopoulos, J.; Wang, W.; Sidarth, S. R.; Foerster, H.; Fruede, D.; Hunger, M. *Phys. Chem. Chem. Phys.* **2005**, *7*, 3221.
(70) Schwager, M.; Dilger, H.; Roduner, E.; Reid, I. D.; Percival, P. W.; Baiker, A. *Chem. Phys.* **1994**, *189*, 667.
(71) Roduner, E.; Prassides, K.; Macrae, R. M.; Thomas, I. M.; Niedermayer, C.; Binninger, U.; Bernhard, C.; Hofer, A.; Reid, I. M. *Chem. Phys.* **1995**, *192*, 231.
(72) Sousa, Goncalves, A. J.; Portsmouth, R. L.; Alexander, P.; Gladden, L. F. *J. Phys. Chem.* **1995**, *99*, 3317.